RAPID LEAF FALLING 1 facilitates chemical defoliation and mechanical harvesting in cotton.

Bing Zhang[1, 6], Dandan Yue[1, 6], Bei Han[1], Danfan Bao[1], Xiao Zhang[1], Xuyang Hao[1], Xin Lin[1], Keith Lindsey[2], Longfu Zhu[1], Shuangxia Jin[1], Maojun Wang[1], Haijiang Xu[3], Mingwei Du[4], Yu Yu[5, *], Xianlong Zhang[1, *], Xiyan Yang[1, *]

[1]National Key Laboratory of Crop Genetic Improvement, Huazhong Agricultural University, Wuhan, Hubei 430070, P. R. China.

[2]Department of Biosciences, Durham University, South Road, Durham DH1 3LE, UK.

[3]Institute of Economic Crops, Xinjiang Academy of Agricultural Sciences, Urumqi, 830091，Xinjiang, P.R. China

[4]College of Agriculture and Biotechnology, China Agricultural University, Beijing 100193, China

[5]Xinjiang Academy of Agriculture and Reclamation Science, Cotton Institute, Shihezi 832000, Xinjiang, P. R. China

[6]These authors contributed equally to this article.

***Correspondence: Xiyan Yang (yxy@mail.hzau.edu.cn)**

Xianlong Zhang (xlzhang@mail.hzau.edu.cn)

Yuyu (xjyuyu021@sohu.com)

ABSTRACT

Chemical defoliation stands as the ultimate tool in enabling the mechanical harvest of cotton, offering economic and environmental advantages. However, the underlying molecular mechanism that triggers leaf abscission through defoliant action remains unsolved. In this study, through single-nucleus mRNA sequencing (snRNA-seq) of the abscission zone (AZ) from cotton petiole, we meticulously constructed a transcriptomic atlas and determined two newly-formed cell types, abscission cells and protection layer cells after defoliant treatment in cotton petiole AZ. *GhRLF1* (Rapid Leaf Falling), which encodes a cytokinin oxidase/dehydrogenase, was identified as key marker gene unique to the abscission cells following defoliant treatment. Overexpression of *GhRLF1* resulted in reduced cytokinin accumulation, accelerating leaf abscission and an enhanced sensitivity to defoliant. Conversely, CRISPR/Cas9-mediated loss of *GhRLF1* function appeared to delay this process. Its interacting regulators, GhWRKY70, acted as pioneer activator, and GhMYB108, acted as successor activator, orchestrate a sequential modulation of *GhRLF1* within the AZ. *GhRLF1* is involved not only in regulating chemical defoliation but also in regulating yield traits, due to its expression pattern in multiple tissue. Finally, transgenic lines exhibiting rapid leaf fall but unaffected cotton yield were developed, using defoliant-induced petiole-specific promoter *proPER21* driving *GhRLF1* (*proPER21::RLF1*). These lines produced equal yield but high defoliation rate, or less defoliation application for mechanical harvesting compared to the control line. This pioneering biotechnological strategy supports a new strategy for chemical defoliation of machine-harvested cotton plants, ensuring stable production and decreasing leaf debris in harvested cotton with an enhanced environmental impact.

Key words: Chemical defoliation; snRNA-seq; Abscission; Machine-harvested cotton

INTRODUCTION

The mechanical harvesting represents the ultimate stage of full mechanization in cotton production. Nevertheless, the elevated impurity rate of machine-harvested cotton poses a bottleneck issue in enhancing the efficiency of cotton cultivation. Chemical defoliation is the passive abscission of leaves at the petiole of metabolically active functional leaves under the action of defoliants to facilitate mechanical clean cotton harvest. The defoliants used in production mainly consist of ethylene and thidiazuron, possessing the functions of defoliation and ripening. Ethylene promotes the endogenous ethylene production and accelerates organ senescence; its ripening effect is superior to its defoliation effect. Thidiazuron is a widely used defoliant that can stimulate rapid cell division and separation; its defoliation effect is superior to its ripening effect. The mixture of thidiazuron and ethylene can enhance boll opening, leaf abscission, and initial harvest more effectively. Organ abscission occurs at a specific structure known as the abscission zone, which has defined boundaries with neighboring cell types and is typically quiescent, subject to precise regulation by developmental and environmental cues. The response of plant varieties to defoliants, and whether they subsequently form abscission zone, is a core factor. Most cotton varieties are not sensitive to defoliants; after defoliant application, the leaves dry up but do not fall off, resulting in a high impurity rate during mechanical harvesting. Current studies focus more on defoliant formulation, application techniques, and physiological mechanisms, with few reports on the formation molecular mechanism of petiole abscission. Therefore, further research is needed to elucidate the intricate transcriptional regulatory mechanisms, interactions between hormone signaling pathways, and precise cellular locations involved in this process. A comprehensive understanding of these mechanisms holds the potential to enhance plant sensitivity to chemical defoliants, further revolutionizing the efficiency of crop harvesting.

Organ abscission is precisely coordinated and finely regulated by phytohormones and other signals (Cheng et al., 2022; Cho et al., 2008; Meng et al., 2016; Patharkar and Walker, 2015; Shi et al., 2011; Stenvik et al., 2008; Yu et al., 2020). Once the AZ is formed, phytohormones can act as distal signals to initiate the abscission process (Liang et al., 2020). For instance, ethylene and auxin are two types of hormones that have been well-studied, whereby auxin can be transported through the AZ, delaying the response of AZ cells to ethylene signals (Chakrabarti and Bharti, 2023; Liang *et al.*, 2020). The occurrence of abscission also involves ethylene-independent regulatory pathways, such as the IDA (Inflorescence deficient in abscission) and PSK peptide hormone-mediated abscission pathways. Previous studies have demonstrated that cytokinins (CKs) have distinct effects on organ senescence and abscission (Lim et al., 2003; Wu et al., 2017), whereby they act as inhibitors of organ senescence (Hönig et al., 2018). Overexpression of isopentenyl transferase

(IPT) under the control of promoter of the senescence-related gene *SAG12*leads to increased cytokinin accumulation, resulting in delayed flower organ senescence (Chang et al., 2003). The level of cytokinins is regulated by the balance between their biosynthesis, inactivation, reactivation, and degradation by cytokinin oxidases, with the CKX gene encoding cytokinin oxidase being a critical target for controlling cytokinin levels. However, in the context of organ abscission, the exogenous application of cytokinins appears to have different effects (Estornell et al., 2013). The regulatory module of the bHLH family transcription factors *RhLOL1-RhILR3* mediates cytokinin-induced floral organ abscission by regulating *AUX/IAA* gene expression (Jiang et al., 2023). Applying exogenous benzylaminopurine (BA) to apple trees stimulates vegetative growth, intensifies competition for nutrients among young fruits, and leads to fruit drop.Currently, our understanding of the response of cotton petioles to chemical defoliant-induced petiole abscission is limited to the discovery that cytokinin synthesis and degradation pathways may play a significant role (Xu et al., 2019). However, the mechanism underlying the response of the petiole AZ to chemical defoliant and the impact of defoliants on cytokinin homeostasis have not been fully elucidated.

Recent breakthroughs in high-throughput single-cell RNA sequencing (scRNA-seq) technology have unleashed a new era of scientific exploration, empowering us to unravel the intricate molecular tapestry of tissues and organs with unprecedented precision (Chen et al., 2021; Gala et al., 2021; Graeff et al., 2021; Kim et al., 2021; Ortiz-Ramirez et al., 2021; Qin et al., 2022; Schaum et al., 2018; Wang et al., 2023a; Wendrich et al., 2020; Zhu et al., 2023). However, the enigmatic realm of cotton AZ remains largely uncharted territory in terms of scRNA-seq studies. This can be attributed to the formidable barriers posed by the robust cell walls that interlock cotton cells, coupled with larger cell sizes. Alternatively, a promising approach known as single-nucleus mRNA sequencing (snRNA-seq) allows transcriptomic analysis at the individual cell level in plants and has recently been applied to soybean nodules, Arabidopsis seeds, maize leaves, and Arabidopsis roots (Farmer et al., 2021; Habib et al., 2016; Liu et al., 2023b; Long et al., 2021; Sun et al., 2022). However, there are currently no reports on the application of snRNA-seq in the petiole of cotton.

Determining the fate determinant factors that govern the induction of cotton petiole abscission by chemical defoliants is potentially economically and environmentally important, as indicated above. We utilized snRNA-seq to create a transcriptomic atlas and discovered *GhRLF1* as a major regulator of cell fate in the AZ. This allowed us to establish the molecular mechanism through which chemical defoliators activate the GhWRKY70/GhMYB108-GhRLF1 module, thereby regulating petiole abscission. Additionally, we discovered the advantageous expression promoter *proGhPER21* in the AZ and showed how this promoter can be used to drive enhanced sensitivity to chemical defoliants in transgenic plants.

RESULTS

The dynamics of the AZ after defoliant treatment for machine-harvested cotton

In our present study, we observed the petioles of Xinluzao50 plants (X50, a cotton variety sensitive to defoliant) at various time points after the application of defoliant (with 10% thidiazuron and 40% ethephon as the active ingredients) (**Figure 1A**). At 72 hours after defoliant treatment, distinct AZs were observed at the base of the petiole (**Figure 1B**). Longitudinal paraffin sectioning revealed that the abscission zone, where the base of cotton petioles was induced to fracture by defoliants, was situated within approximately 10 cell layers in the middle between the elongated and large cells at the distal end and the flattened and small cells at the proximal end (**Figure 1C**). Moreover, the fracture zone began to form 48 hours after defoliant treatment (**Figure 1C**). As the petiole responds to chemical defoliants, scanning electron microscopy (SEM) was employed to examine the transverse fracture plane of the petiole. It was observed that nearly all cells exhibited a uniform fracture state prior to 24 hours of treatment; however, after 48 hours, fracture zones began to develop, with abscission cells appearing rounded and turgid. Subsequently, the number of abscission cells increased progressively alongside an expansion of the fracture zone until complete disintegration occurred (**Figure 1D**). Furthermore, as the abscission process advanced, these abscission cells gradually differentiated into protective layer cells, thereby enhancing their resilience against external environmental factors (**Figure 1D**). Based on these findings, we propose a working model for the development of cotton abscission cells and a protective layer (**Figure 1E**).

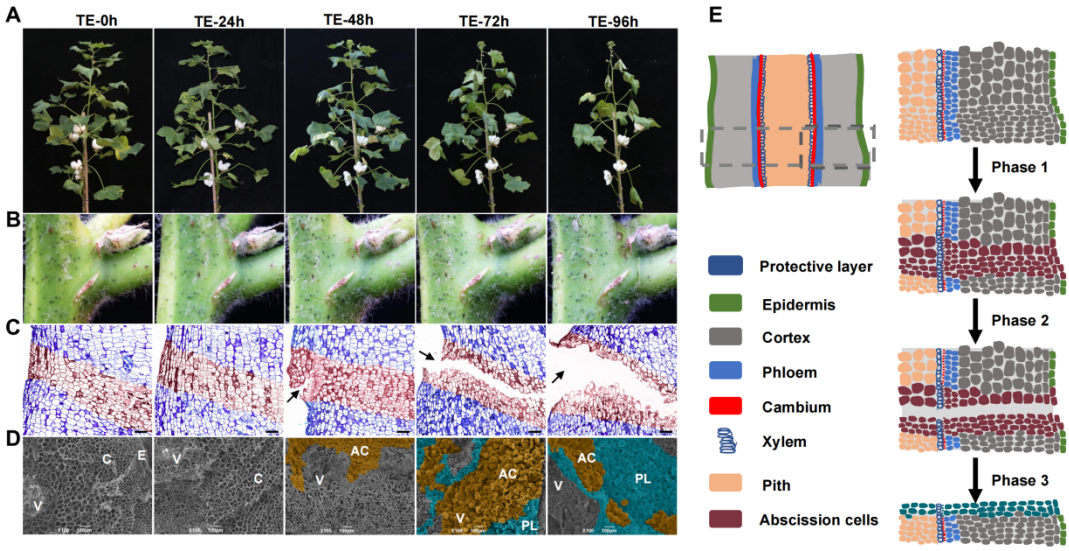

Figure 1 The dynamics of the abscission zone (AZ) after defoliant treatment in cotton petioles.

(A and B) Representative images of cotton plants (A) and base of petiole (B) at 0, 24, 48, 72, and 96 hours after defoliant treatment. (C) Longitudinal sections of the AZ region of cotton plants at 0, 24, 48, 72, and 96 hours after defoliant treatment. The formation of an AZ is indicated by the black arrow. Brown indicates the position where future petiole abscission will take place. The sections were stained with toluidine blue. Bars = 50 μm. (D) Cross-sections of the AZ observed by scanning electron microscopy (SEM) at 0, 24, 48, 72, and 96 hours after defoliant treatment. Epidermis (E), cortex (C), vascular bundles (V) abscission cells (AC), and protective layer (PL). AC and PL are indicated in yellow and blue, respectively. Bars = 100 μm. (E) Schematic diagram of longitudinal section of the base of a cotton petiole showing the spatial distribution of cell clusters in AZ region and the dynamic change during the process of abscission. The right part is a magnified view of the shaded part on the left.

Two newly-formed cell types, abscission cells and protection layer cells determined by snRNA-seq in the AZ after defoliant treatment

To investigate the molecular mechanism controlling AZ cell fate, we used snRNA-seq to generate a comprehensive transcriptional profile of the major cell types within the AZ before and at various time points after defoliant treatment. Approximately 100,000 nuclei per sample were then processed for droplet-based snRNA-seq using the 10× Genomics snRNA-seq platform (**Supplemental Table 1**). The results of quality control analysis showed high reproducibility between the biological replicates (**Supplemental Figures 1A and 1B**). Fourteen cell clusters were identified in each of the two datasets, clusters 0 to 13 in the X50_0 dataset (before defoliant treatment), and clusters 0-9, 11, 14-16 in the X50_all dataset (after defoliant treatment) (**Figures 2A and 2B; Supplemental Figures 2A and 2B**). The top 50 highly expressed genes for each cell cluster were used to determine the cell types for cotton petiole AZ (**Supplemental Tables 2 and 3**). This analysis divided those cell clusters into 7 cell types, with two newly-formed cell types, abscission cells (cluster 14) and protection layer (cluster 15 and 16) appearing in the X50_all dataset (**Figures 2A and 2B**), and the cell numbers in the clusters 14 and 16 increased as post-treatment time went on (**Supplemental Figure 2C**).

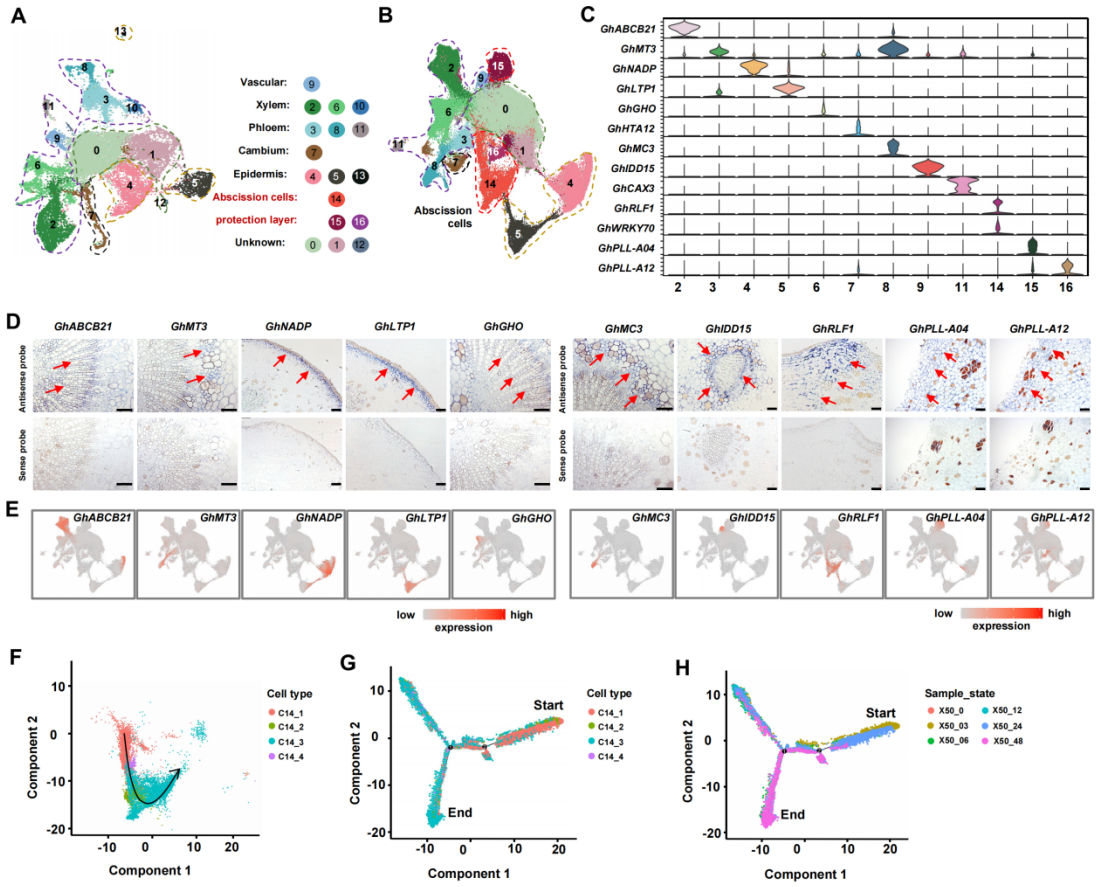

Figure 2 Cell atlas and cluster annotation of single-cell transcriptomes from cotton petioles.

(A and B) UMAP visualization of 14 cell clusters (0-13) in the X50-0 (before treatment) (A) and 14 clusters (0-9, 11, 14-16) in the X50-All (before and after treatment) (B). Each dot indicates a single cell. Different numbers and colors denote different cell clusters. Clusters 0, 1, and 12 represent unknown cells; clusters 2, 6 and 10 represent xylem cells; clusters 3, 8 and 11 represent phloem cells; cluster 7 represents cambium cells; clusters 4, 5 and 13 represent epidermis cells; cluster 9 represents vascular cells; clusters 14 represent abscission cells; and cluster 15 and 16 represents protective layer cells. See Supporting Information Supplemental Tables 2 and 3 for details of the enriched genes in each cluster. (C) Violin plots showing the expression patterns of cell type-specific marker genes in different clusters. Clusters are indicated on the x-axis. The colors denote the corresponding cell clusters. (D) RNA in situ hybridization of 10 marker genes in different clusters. The red arrows show the signals. Bars = 100 μm. (E) UMAP plot showing the distribution and expression levels of 10 marker genes in different clusters. Gray represents low expression levels, and red represents high expression levels. (F-H) Pseudotime trajectory showing the development of abscission cells (cluster 14). UMAP projections showing abscission cells populations. C14_0 to C14_4, sub-cell clusters (F). The horizontal and vertical coordinates are two principal components, and the dots represent different cells. Different colors represent the sub-cell clusters (F and G) or the cells

from each period (H).

The top 5 highly expressed genes were defined as marker genes for each cell types (**Supplemental Figures 2D-G**), and the expression profiles of some marker genes were visualized to illustrate their cell type-specific pattern by snRNA-seq data and RNA in situ hybridization (**Figures 2C-E**). For instance, *ABCB21* (Ghir_A12G012980, in cluster 2), and *GHO* (Ghir_A05G019870, in cluster 6) exhibited preferential expression in the xylem; *MT3* (Ghir_A11G031060, in cluster 3 and cluster 8) and *MC3* (Ghir_A01G001300, in cluster 8) in the phloem; *IDD15* (Ghir_D11G000260, in cluster 9) in the vascular bundle sheath; *NADP* (Ghir_D12G018390, in cluster 4), *LTP1* (Ghir_A10G015260, in cluster 5) in the epidermis; *RLF1* (Ghir_A07G001250, in cluster 14) in the newly-formed abscission cells; and *PLL-A04* (Ghir_A04G014810, in cluster 15), and *PLL-A12* (Ghir_A12G019870, in cluster 16) in the protection layer cell (**Figure 2D**). These findings confirm the significant degree of cell heterogeneity in the cotton petiole AZ. The abscission cells were re-clustered and divided into four sub-cell clusters, denoted as C14_1 to C14_4 (**Figure 2F**). We applied monocle2 to order the four sub-cell clusters along a reconstructed trajectory of abscission cell development. The inferred trajectories revealed gradual transitions from cells in C14_1, C14_4, C14_2 to the subcluster C14_3 (**Figure 2G and Supplemental Table 4**). Additionally, the pseudo-time and true-time development exhibited consistent patterns (**Figures 2F-H**).

The process of abscission involves alterations in cytokinin, auxin and ethylene contents and cell wall loosening, and the defoliant used reduces cytokinin levels and increases ethylene production and associated genes, although the cell types in which these changes occur have not been identified previously (Li et al., 2022). Gene Ontology (GO) analysis was performed using the expressed genes in different cell types, and as anticipated, the majority of the enriched terms or pathways were associated with the cell type of interest (**Supplemental Figures 3A-C**). For example, genes in abscission cells exhibited enrichment of terms associated with cytokinin catabolic processes, salicylic acid-mediated signaling, pectate lyase activity, and pectin catabolic processes (**Supplemental Figures 3A and 3B**). hdWGCNA was performed on the core abscission cell population (**Supplemental Figure 4A**). Notably, one module was found to be rich in cytokinin pathway genes, with *RLF1* at its core (**Supplemental Figure 4B**). In addition, genes associated with the auxin and ethylene pathways were involved in the response to chemical defoliant induction. The expression levels of auxin-related genes were reduced upon defoliant induction, while ethylene-related genes showed initial upregulation followed by a gradual decrease toward preinduction levels (**Supplemental Figure 4C**). These findings further support the pivotal role of plant hormone metabolism pathways in the process of cotton petiole abscission induced by defoliants.

Abscission cell-specific *GhRLF1* is a superior driver for cotton leaf abscission

GhRLF1 (Ghir_A07G001250), the most highly expressed of the core components of abscission cell cluster 14, with its homologous genes Ghir_A13G020630, are inferred to play positive roles in cotton leaf abscission based on snRNA-seq data (**Supplemental Table 3**). Based on the genomic data and defoliation rate phenotype data of a natural population containing 517 cotton germplasm, the natural genetic variation of the two genes mentioned above was analyzed. Some variations were found in the genome sequence of *GhRLF1* (**Figure 3A**), but there was no non synonymous mutation in the coding region of Ghir_A13G020630. There are two haplotypes (hap^G/hap^A) in the population at position 718 amino acid of the *GhRLF1* coding region, and the germplasms containing the hap^G allele displayed a higher defoliation rate than those containing the hap^A allele (**Figure 5B**). Thus, we selected *GhRLF1* for functional analysis.

Two knockout mutants (*rlf1#1* and *rlf1#14*) generated via CRISPR/Cas9-mediated genome editing near the aforementioned SNP loci (**Figure 3C**), and two overexpression lines (*35S::GhRLF1#1* and *35S::GhRLF1#6*) were obtained for enhanced expression of *GhRLF1* (**Figure 3D**). Those lines and wild-type (WT) were selected for characterizing the role of *GhRLF1* in cotton leaf abscission. After 72 hours of defoliant application, all the top leaves of the WT and overexpression plants had already detached from the main body, and the leaves at the 5th and 6th nodes of the overexpression lines were shed earlier than those of the WT (**Figure 3C**); this was not observed for the knockout mutant lines. We also conducted detailed observations on the histological and cytological morphology of these lines. The results showed that after 48 hours of defoliant treatment, the overexpression lines (*35S::GhRLF1#1* and *35S::GhRLF1#6*) exhibited an accelerated the formation of abscission cells and fracture zones compared to that of the wild type. In contrast, the knockout mutants (*rlf1#1* and *rlf1#14*) had the opposite effect (**Figure 6E and 6F**). Similarly, the rate of leaf abscission and the expression level of *GhRLF1* also followed this pattern (**Figures 3G and 3H**). Taken together, these results ultimately indicate that GhRLF1 promotes the response of cotton plants to defoliants by accelerating leaf abscission via upregulated expression.

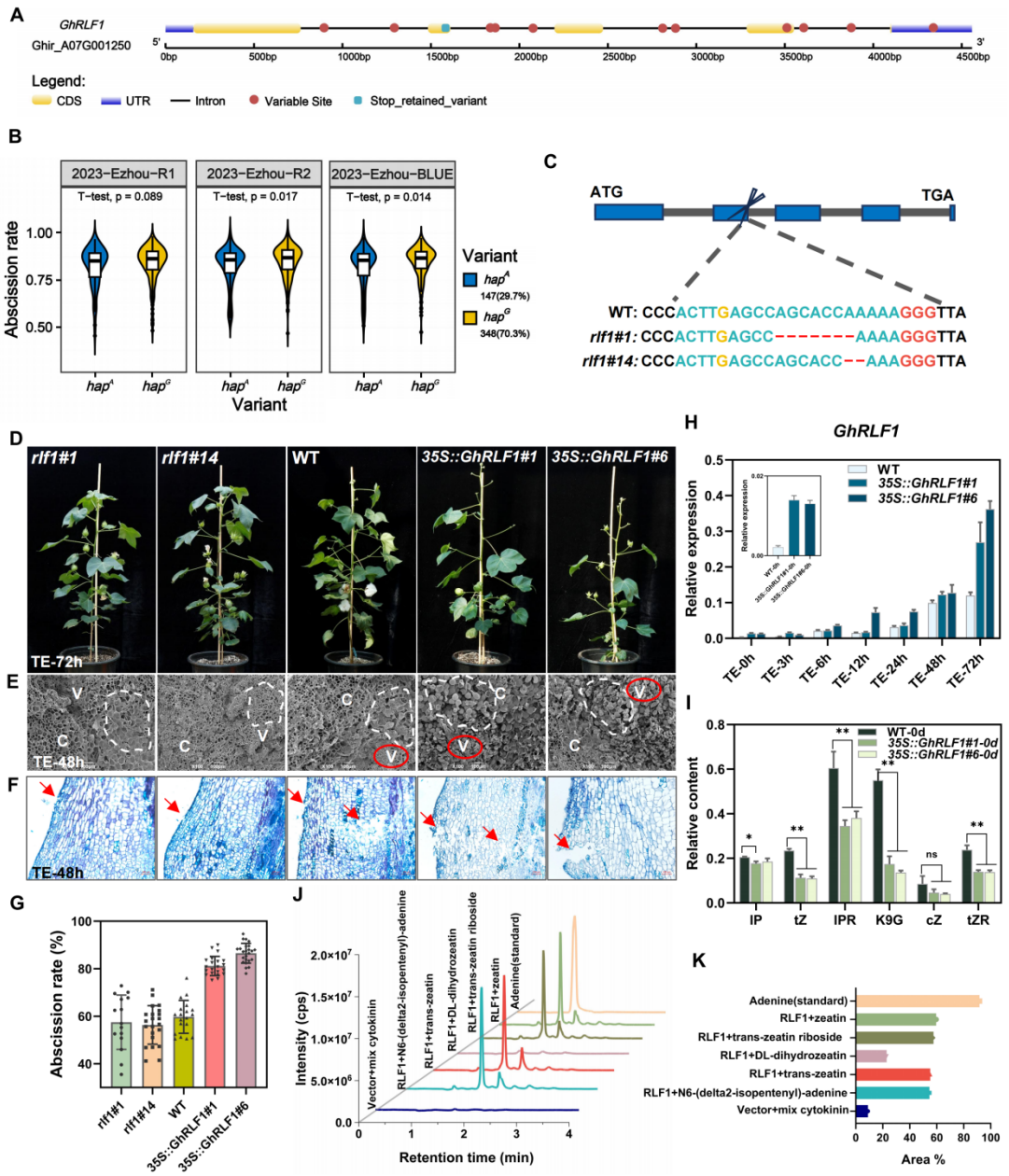

Figure 3 *GhRLF1* positively regulates chemical defoliation in cotton.

(A) Distribution of genomic variation sites in GhRLF1 (Ghir_A07G001250). (B) The degree of association between different homozygous haplotypes (hapG/hapA) and defoliation phenotype. (C) Detection of editing efficiency for *rlf1#1* and *rlf1#14*. The yellow font base G is the location of SNP variation in the natural population mentioned above. (D) Phenotypes of the wild-type and transgenic lines after 72 hours of chemical defoliant application. *35S::GhRLF1#1* and *35S::GhRLF1#6* are overexpression lines, and *rlf1#1* and *rlf1#14* are knockout mutant lines. (E) show scanning electron microscopy images of the fracture plane in the wild-type and transgenic lines after 48 hours of defoliant treatment, during manual removal. Epidermis (E), collenchyma (Col), cortex (C), and vascular bundles (V). The scale bars in 100X represent 100 μm. (F) The longitudinal images of the petiole abscission zone in

the wild-type and *GhRLF1* transgenic lines at 48 hours after defoliant treatment. Bars = 1000μm. The formation of an AZ is indicated by the red arrow. (G) The defoliation rates of wild-type and transgenic lines after four days of defoliating agent application. The values in (G) are the means ± SEs (n >= 10). (H) The relative expression levels of *GhRLF1* in the petiole AZ of the wild-type and overexpression plants were measured at various time points after defoliant treatment. The values in (H) were determined using RT–qPCR and are presented as the means ± SEs (n = 3). GhUB7 was used as an internal reference. (I) Relative content of several endogenous cytokinins in the petiole AZ. N6-(delta 2-isopentenyl)-adenine (IP), trans-zeatin (tZ), N6-isopentenyladenosine (IPR), kinetin-9-glucoside (K9G), cis-zeatin (cZ), and trans-zeatin riboside (tZR). The values in (I) are the means ± SEs (n = 3), and significant differences were analyzed using Student's t test; ** indicates $P<0.01$, * indicates $P<0.05$ and ns indicates not significant. (J) High-performance liquid chromatography (HPLC) diagram showing the degradation of various cytokinins by the GhRLF1 protein in vitro. The amount of cytokinin used in the experimental group remained consistent. Adenine (Ade) was used as a product standard and served as a positive control. (K) The peak area corresponding to each peak in (J) is displayed.

The GhRLF1 protein contains a cytokinin-binding domain, which may degrade cytokinin irreversibly and regulate cytokinin homeostasis (Zeng et al., 2022; Zhao et al., 2015). Based on these findings, we measured the levels of more than ten different types of endogenous cytokinin in the cotton petiole AZ. The results revealed that overexpression of *GhRLF1* led to a reduction in the cytokinin content within the plant (**Supplemental Figure 5A**). By inducing the expression and purifying the GhRLF1 protein in vitro, and using five types of cytokinins (zeatin (CZ), trans-zeatin (tCZ), DL-dihydrozeatin (DHZ), N6-(delta2-isopentenyl)-adenine (2-IP), and trans-zeatin-ribose (tZR)) as substrates, we detected the production of the reaction product adenine (Ade) through HPLC. The results confirmed that GhRLF1 possesses cytokinin oxidase activity in vitro, but there are variations in its ability to degrade different types of cytokinins. Notably, GhRLF1 exhibited a greater ability to degrade zeatin and a weaker ability to degrade DL-dihydrozeatin (**Figures 3J and 3K and Supplemental Figures 6B and 6C**). These findings further confirmed that increased expression of *GhRLF1* can reduce cytokinin content and disrupt cytokinin homeostasis in the AZ and this gene could be used as a genetic tool to increase sensitivity to chemical defoliants.

Defoliants induced GhWRKY70 activates the expression of *GhRLF1* in abscission cells, thereby accelerating the abscission process

Proteins containing 1 cytokinin-binding domain can act as a downstream target for transcriptional activation (Gao et al., 2014; Geng et al., 2022). These findings prompted us to

confirm whether a similar transcriptional regulatory mechanism exists in abscission cells. We found that a WRKY family transcription factor *GhWRKY70* exhibited strong co-expression with *GhRLF1* (**Figure 4A**). In situ hybridization results showed that the hybridization signals of *GhWRKY70* (Ghir_A05G028330) and *GhRLF1* were similar (**Figure 2D and Figures 4B and 4C**).

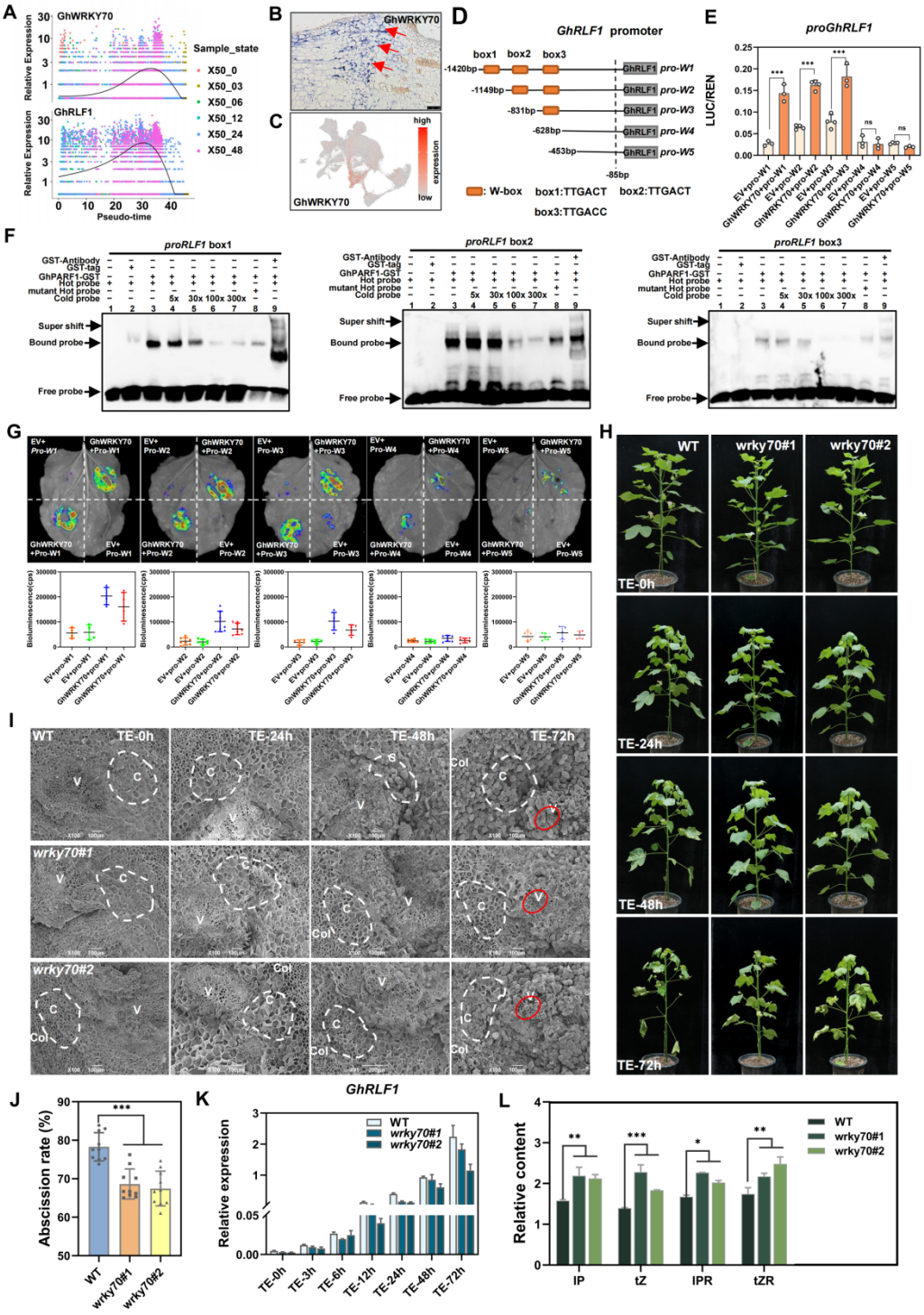

Figure 4 GhWRKY70 activates the expression of *GhRLF1* in abscission cells after

defoliant treatment and positively regulates chemical defoliation in cotton.

(A) Pseudotime and relative expression levels of *GhWRKY70* and *GhRLF1* in the detached area of the petiole after defoliant treatment. (B) In situ hybridization of *GhWRKY70*; the arrow indicates the position at which the signal was enriched. (C) UMAP map of snRNA-seq data showing the enrichment location of *GhWRKY70*. Bars = 100 μm. (D) Distribution of W-boxes within the *GhRLF1* promoter sequence. The truncated pro-W1 to pro-W5 promoter sequences were generated by sequentially truncating a W-box from the 5′-end of the promoter and used for subsequent dual-luciferase reporter assays. (E) Transient dual-luciferase reporter assays in cotton (YZ1) protoplasts. The ratio of firefly luciferase (LUC) to Renilla luciferase (REN) reflects the *GhWRKY70* activation ability. The values represent the means ± SEs (n >= 3), and significant differences were analyzed using Student's t test; *** indicates P<0.001, and ns indicates not significant. (F) EMSA of the DNA binding activity of GhWRKY70 to the *GhRLF1* promoter. Box1, box2 and box3 were labeled with biotin as hot probes and incubated with the GhWRKY70-GST recombinant protein. Unlabeled probes were added as cold probes at a concentration gradient much higher than that of the hot probes to compete for protein binding. The mutation probes served as controls. The empty GST tag carrier served as a negative control. GST antibodies are used to bind proteins and DNA-binding complexes. (G) Transient dual-luciferase reporter assays in tobacco leaves. The bioluminescence intensity and numerical value reflect the strength of the binding of GhWRKY70 to the *GhRLF1* promoter. EV represents the empty pGreenII 62-SK vector, used as a control. The data in (G) was the means ± SEs (n >= 4 leaves). (I) Scanning electron microscopy image of the fracture plane of the wild-type and *GhWRKY70* knockout mutant plants after manual removal of petioles at different time points during defoliant treatment. Epidermis (E), collenchyma (Col), cortex (C), and vascular bundles (V). The scale bar at 100× indicates 100 μm. (J) The defoliation rates of wild-type and knockout mutants after four days of defoliating agent application. The values in (J) are the means ± SEs (n = 10). (K) The relative expression levels of *GhRLF1* in the petiole AZ of the wild-type and knockout mutants were measured at various time points after defoliant treatment. The values in (K) were determined using RT–qPCR and are presented as the means ± SEs (n = 3). GhUB7 was used as an internal reference. (L) Relative content of several endogenous cytokinins in the petiole AZ. N6-(delta 2-isopentenyl)-adenine (IP), trans-zeatin (tZ), N6-isopentenyladenosine (IPR), and trans-zeatin riboside (tZR). The values in (L) are the means ± SEs (n = 3), and significant differences were analyzed using Student's t test; *** indicates P<0.001, ** indicates P<0.01, and * indicates P<0.05.

WRKY proteins are typical nuclear localized transcription factors that contain a nuclear localization sequence (NLS) (Robatzek and Somssich, 2001). The conserved WRKY domain can recognize and bind to the W-box, with a core motif of (T)TGAC(C/T) (Chi et al., 2013;

Huang et al., 2010). We analyzed the possible W-boxes approximately 1.5 kb upstream of *GhRLF1* and ultimately identified three W-boxes (**Figure 4D**). Through a luciferase (LUC) assay and an electrophoretic mobility shift assay (EMSA), we found that *GhWRKY70* strongly activates *GhRLF1* (**Figures 4E-G**). In detail, EMSA confirmed that the recombinant GST-labeled fusion protein (GST-GhWRKY70) was capable of binding to the W-box on the *GhRLF1* promoter, whereas the binding ability of the mutant probes was significantly diminished (**Figure 4F**). Furthermore, we validated the specificity of GhWRKY70 for binding to the *GhRLF1* promoter by utilizing a GST antibody to decrease the electrophoretic migration rate and generate supershifted bands after binding to the protein-probe complex (**Figure 4E**). These results indicate that *GhWRKY70* activates the transcription of *GhRLF1* in cotton petiole abscission cells.

We generated wrky*1/2* mutant lines that underwent base insertion (**Supplemental Figure 6A**). In comparison to wild-type, the knockout mutants exhibited reduced sensitivity to defoliants and demonstrated a delay in leaf abscission, with no significant signs of leaf abscission observed at 48 hours (**Figure 4H**). Furthermore, SEM revealed that at 48 hours, the abscission cells appeared in the wild-type group, while most of the cells in the knockout mutants group remained fragmented until 72 hours, when complete abscission cells gradually formed on the fracture plane (**Figure 4I**). At this time, the abscission cells almost filled the fracture plane of the wild-type plants, and there were almost no broken cells in the vascular bundle (**Figure 4I**). The results of abscission rate and the longitudinal paraffin sectioning likewise demonstrated that the knockout mutants delayed leaf abscission (**Figure 4J and Supplemental Figure 6B**). Lastly, through the examination of *GhRLF1* expression levels in the petiole abscission zone of both the knockout mutants and wild-type, alongside the assessment of several major endogenous cytokinins, it was observed that *GhRLF1* expression in the petiole abscission zone of the knockout mutants were significantly reduced (**Figure 4K**). In contrast, the levels of several key endogenous cytokinins exhibited a notable increase (**Figure 4L**). These results suggest that *GhWRKY70* plays a pivotal role in activating the transcription of *GhRLF1* in cotton petiole abscission cells. Furthermore, mutations in *GhWRKY70* may diminish the sensitivity of cotton plants to defoliants, subsequently delaying the abscission process of cotton petiole cells.

GhMYB108 acts as a late activator of *GhRLF1* in AZ of cotton petiole after defoliant treatment

After 48 hours of defoliant treatment, the expression of *GhWRKY70* significantly decreased, while the expression of *GhRLF1* continued to increase (**Figure 5A**). This discovery prompted us to test whether cytokinin signaling affects the transcription level of *GhWRKY70*. Previous studies have shown that cytokinin signaling can promote the accumulation of WOX11 protein in the root apical meristem of rice ((Geng *et al.*, 2022)). First, we tested the effect of

application of 1μM 6-BA on WRKY70 protein accumulation and transcript levels during time courses. Immunoblot data and RT-qPCR revealed that, compared to the control, WRKY70 protein and transcript levels significantly increased 15 min after 6-BA treatment (**Supplemental Figures 7A-C**). Importantly, the expression level of *GhWRKY70* was reduced in the petiole of 35S::RLF1, and conversely in knockout mutant (**Supplemental Figure 7D**). Thus, endogenous cytokinins may promote the expression of *GhWRKY70*. The sustained increase in the expression level of *GhRLF1* prompted us to consider whether other transcription factors play crucial roles in the later stages of the abscission process. We conducted further analysis of the snRNA-seq data and found that the expression profile of a MYB family transcription factor gene *GhMYB108* (Ghir_D02G006060) in clusters associated with protective layer formation, such as clusters 2, 6, and 16, closely resembled that of *GhRLF1* (**Supplemental Figure 8**), and it was upregulated after 48 hours of defoliant treatment (**Figure 5A**). It was speculated that GhMYB108 might play a role in the later stages of cotton petiole abscission. We analyzed the region approximately 2 kb upstream of *GhRLF1* and identified seven MYB binding sites, which were subsequently truncated (**Figure 5B**). LUC assays revealed that GhMYB108 bound to the promoter of *GhRLF1* and activated its transcription unless the promoter sequence was truncated to the remaining sequence without MYB binding sites (proM7) (**Figure 5C and Supplemental Figure 9**). Furthermore, a yeast one-hybrid (Y1H) assay showed that Bait-M7 and Bait-M8 were able to grow on media without the addition of the antibiotic AbA, but their growth was significantly inhibited on media supplemented with 500 ng/ml AbA. However, GhMYB108 was able to interact with other bait sequences (**Figure 5D**). Additionally, EMSA revealed that GhMYB108 can bind to possible MYB binding sites(**Figure 5E**). In summary, GhMYB108 can bind to the *GhRLF1* promoter sequence and activate its expression.

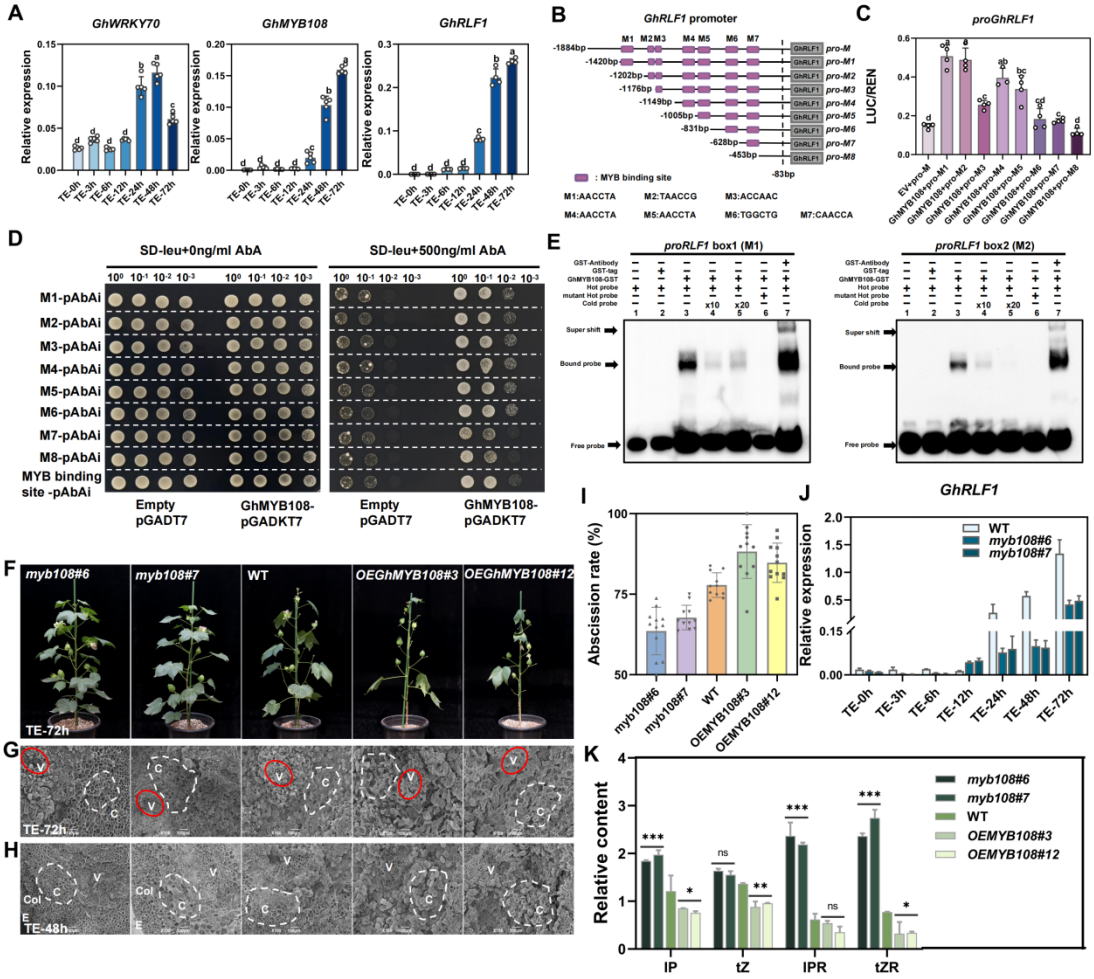

Figure 5 GhMYB108 acts as a successor activator of GhRLF1 in AZ of cotton petiole after defoliant treatment.

(A) Expression patterns of *GhWRKY70*, *GhMYB108* and *GhRLF1* at different time points after defoliant treatment. The values represent the means ± SEs (n >= 4), and significant differences were analyzed using multiple comparisons. (B) Distribution of MYB binding sites within the *GhRLF1* promoter sequence. The truncated promoter sequences pro-M1 to pro-M8 were generated by sequentially truncating a MYB binding site from the 5′-end of the promoter and subsequently used for dual-luciferase reporter assays. (C) Transient dual-luciferase reporter assays in cotton (YZ1) protoplasts. The ratio of firefly luciferase (LUC) to Renilla luciferase (REN) reflects the activation ability. The values represent the means ± SEs (n >= 3), and significant differences were analyzed using multiple comparisons. (D) Yeast-one-hybrid (Y1H) assays revealed that GhMYB108 could bind to the *GhRLF1* promoter region. Interactions were determined on selective media lacking Leu in the presence of 500 ng ml^{-1} aureobasidin A (SD/−Leu + 500 ng ml^{-1}AbA). Different colonies of yeast represent different dilution times. (E) EMSA of the binding of GhMYB108 to the *GhRLF1* promoter. M1 and M2 were labeled with biotin as hot probes and incubated with the recombinant GhMYB108-GST protein. Unlabeled probes were added as cold probes at a

concentration gradient much higher than that of the hot probes to compete for protein binding. The mutation probes served as controls. The empty GST tag carrier served as a negative control. GST antibodies are used to bind proteins and DNA-binding complexes. (F) Phenotypes of the wild-type and transgenic lines after 72 hours of chemical defoliant application. myb108*#6* and myb108*#7* are knockout mutant lines. *OEGhMYB108#3* and *OEGhMYB108#12* are overexpression lines. (G and H) are scanning electron microscopy images of the fracture planes of wild-type and transgenic lines treated with defoliants after 48 hours and 72 hours, respectively, during manual removal. The scale bar at 100× represents 100 μm. (I) The defoliation rates of wild-type and knockout mutants after four days of defoliating agent application. The values in (I) are the means ± SEs (n >= 10). (J) The relative expression levels of *GhRLF1* in the petiole AZ of the wild-type and knockout mutants were measured at various time points after defoliant treatment. The values in (J) were determined using RT–qPCR and are presented as the means ± SEs (n = 3). GhUB7 was used as an internal reference. (K) Relative content of several endogenous cytokinins in the petiole AZ. N6-(delta 2-isopentenyl)-adenine (IP), trans-zeatin (tZ), N6-isopentenyladenosine (IPR), and trans-zeatin riboside (tZR). The values in (K) are the means ± SEs (n = 3), and significant differences were analyzed using Student's t test; *** indicates P<0.001, ** indicates P<0.01, * indicates P<0.05 and ns indicates not significant.

GhMYB108 is upregulated in response to chemical defoliants, but further investigation is needed to determine whether this gene can accelerate cotton leaf abscission. Therefore, we created overexpression lines (*OEGhMYB108#3* and *OEGhMYB108#12*) and knockout mutants with frame-shift mutations (**Supplemental Figure 10A**). After 72 hours of defoliant treatment, the wild-type leaves began to abscise, and almost all the leaves of the overexpression lines had fallen off (**Figure 5F**). However, the knockout mutants exhibited a significant decrease in sensitivity to defoliants (**Figure 5F**). Paraffin sectioning and scanning electron microscopy revealed that the phenotypes of the *GhMYB108* transgenic lines were similar to those of the *GhRLF1* line, with only a slight decrease in the severity of the reaction (**Supplemental Figure 10B and Figures 5G and 5H**). The results of abscission rate in the field are also consistent with the above results (**Figure 5I)**. Furthermore, a reduction in the expression level of *GhRLF1* was observed at the *myb108#6* and *myb108#7* petiole base (**Figure 5J**). Subsequent analysis was performed on the predominant cytokinin levels in the petiole base across all transgenic lines and the wild type. The findings indicated a notable elevation of IP, IPR, and tZR levels in the overexpression lines compared to the wild type, whereas a marginal decline in IP, tZ, and tZR levels was detected in the knockout lines (**Figure 5K**). The above results indicate that GhMYB108 acts as a successor activator positively regulates the expression of *GhRLF1*, thereby positively regulating cotton

defoliation.

***proPER21*::*RLF1* promotes mechanized harvesting by exploiting its predominant expression in the cotton petiole AZ.**

Cytokinins play a significant role in increasing yield, and their activity is negatively regulated by cytokinin oxidase/dehydrogenase (Chen et al., 2020b; Schwarz et al., 2020; Yeh et al., 2015). Our field experiments with *GhRLF1* transgenic lines revealed an intriguing phenotype. We found that, regardless of the developmental stage (0DPA for the ovary, 5DPA, 10DPA, or 15DPA), the ovaries and bolls of the knockout mutant were significantly larger than those of the overexpression lines, while the wild-type plants exhibited an intermediate size (**Figures 6A and 6B**). Consequently, we explored the potential impact of *GhRLF1* overexpression on both yield and quality.

It has been reported that downregulation of the genes encoding cytokinin oxidase/dehydrogenase in cotton carpels can specifically upregulate cytokinins, leading to an increase in cotton seed and fiber yield (Zeng *et al.*, 2022). In our study, we conducted a statistical analysis of the lint and seed cotton weight of 20 cotton bolls, and the results revealed that overexpression of *GhRLF1* not only increased the defoliation rate but also posed significant challenges in terms of yield reduction, which can be attributed to *pro35S* being a strong promoter (**Figure 6C**). Therefore, to improve the defoliation rate without compromising cotton yield or quality, it is crucial to identify suitable promoters. However, the tissue localization of GFP fluorescence in the *proGhRLF1::GFP-GUS* transgenic line was very similar to that in the *pro35S::GFP-GUS* line, indicating that *proGhRLF1* cannot be considered a candidate promoter (**Supplemental Figure 11A**). Based on previous research, we identified another gene, *GhPER21*, which exhibits significant upregulated expression induced by chemical defoliants (Xu *et al.*, 2019). The GFP fluorescence of the *proGhPER21::GFP-GUS* plants indicated that the cross-section of entire abscission area of the petiole exhibits obvious fluorescence signal, while the root hairs showed slight fluorescence (**Supplemental Figure 11B**). The GUS staining results also confirmed that proGhPER21 is predominantly expressed in the AZ region and weakly expressed in the stem (Supplemental Figure 11C). *GhPER21* was expressed at higher levels specifically in the stem and petiole AZ, with highest expression level in petiole AZ, and it exhibited a relative high expression level after defoliant treatment (**Supplemental Figure 11D**). These findings suggest that *proPER21* is AZ-specific and defoliant-induced promoter.

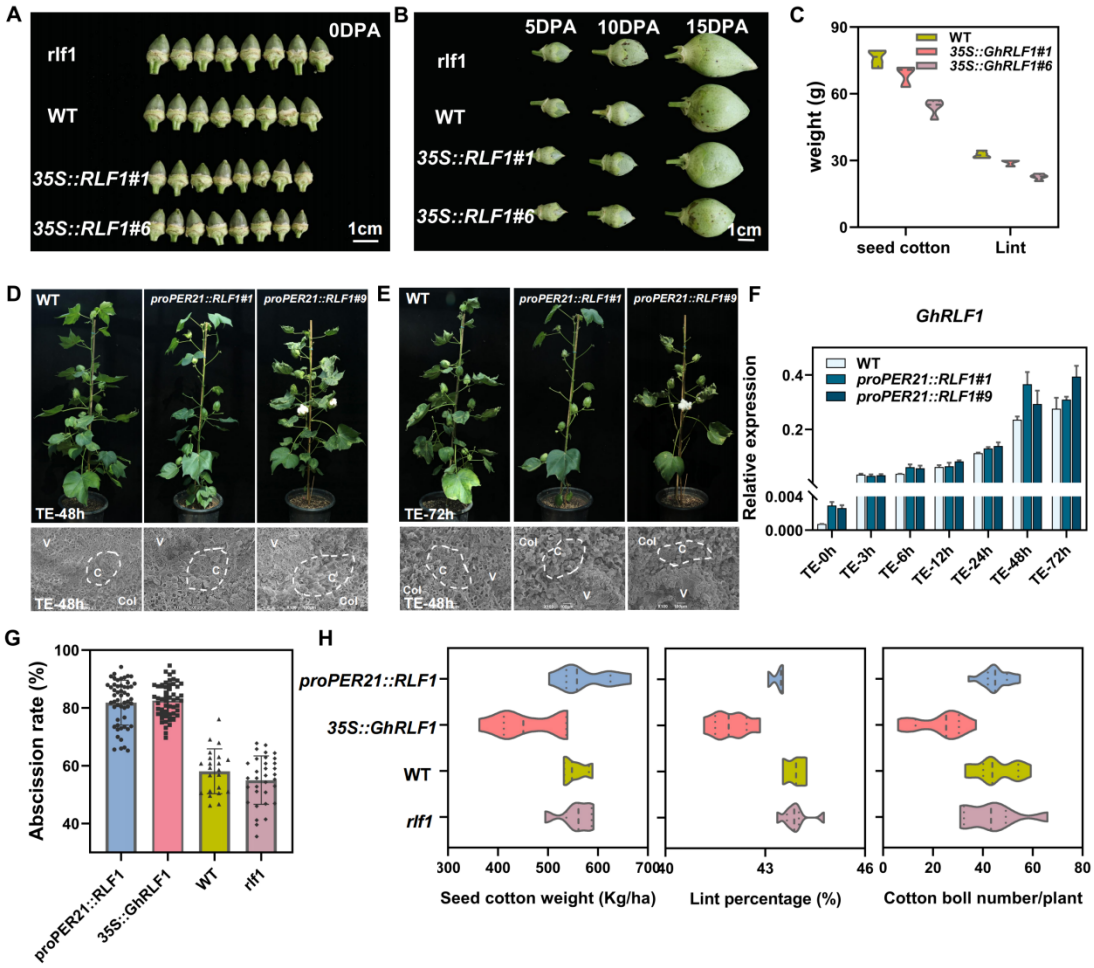

Figure 6 Generation of rapid leaf falling transgenic lines (*proPER21::GhRLF1*) with unaffected cotton yield.

(A) Comparison of ovule size at 0 DPA between the wild-type and *GhRLF1* transgenic lines. Bars = 1cm. (B) Comparison of cotton bolls size at 5 DPA, 10 DPA, 15 DPA between wild-type and *GhRLF1* transgenic lines. Bars = 1cm. (C) The weight of lint and seed cotton from 20 cotton bolls in each of the wild-type and *GhRLF1* transgenic lines. (D and E) Phenotypes of the wild-type and overexpression lines 48 hours and 72 hours after defoliant treatment, as well as scanning electron microscopy images of the AZ. The bars in the scanning electron microscopy image represent 100 μm at 100X magnification. (F) The expression levels of *GhRLF1* in the petiole AZ of cotton petioles were measured in the wild-type and overexpression lines at different time points after defoliant treatment. The values in a were determined using RT–qPCR and are presented as the means ± SEs (n = 3). *GhUB7* was used as an internal reference. (G) Defoliation rates of the wild-type and *GhRLF1* transgenic lines after four days of defoliating agent treatment. The values in (G) are the means ± SEs (n >=20 plants). **(**H**)** Seed cotton weight, lint percentage, and number of bolls per plant of the *GhRLF1* transgenic and wild-type lines.

Therefore, we utilized the *proPER21* promoter to generate the *GhRLF1* transgenic overexpression lines (*proPER21::RLF1#1* and *proPER21::RLF1#9*) (**Figures 6D and 6E**). After 48 hours of defoliant treatment, cracks started to appear in the abscission area of the petiole in the overexpression line, and partial detachment began to occur (**Figure 6D**). By 72 hours, the cells on the fracture surface were fully spherical (**Figure 6E**). The RT–qPCR results demonstrated that *GhRLF1* was highly expressed in *proPER21::RLF1* and was induced by defoliants (**Figure 6F**). The abscission rate of the petiole had significantly increased, and the fracture zone was completely disrupted (**Figure 6G**). Moreover, the size of the cotton bolls from *proPER21::RLF1* was comparable to that of the bolls from the wild type, indicating that the yield reduction associated with *GhRLF1* overexpression was mitigated (**Supplemental Figure 11E**). Furthermore, field experiments were conducted to investigate the sensitivity of transgenic cotton lines overexpressing *GhRLF1* to different concentrations of defoliants during the harvest period. As expected, the overexpression of *GhRLF1* accelerated the response of cotton plants to chemical defoliants; moreover, under treatment with a 70% concentration of the defoliant, the defoliation rate of *GhRLF1* overexpressing lines could reach or even exceed the defoliation rate of the wild type treated with a 100% concentration of the defoliant (**Supplemental Figures 12A-C**). Through examination of yield-related parameters, it was found that the use of the *proPER21* promoter could rescue the yield reduction defect caused by the *35S::GhRLF1* transgene while simultaneously improving defoliation efficiency and stabilizing yield (**Figure 6H**).

DISCUSSION

Plant organ abscission has a high degree of precision, programmability, and complexity (Lee et al., 2018; Lewis et al., 2006; Reichardt et al., 2020; Roberts et al., 2002). Compared to the natural abscission of typical plant organs due to normal growth and development, chemically induced abscission serves as an external intervention to regulate leaf abscission, having certain practicality and urgency for the mechanized harvesting of cotton. This renders this work of significant biological significance. Due to the extremely senescent state of cotton petioles during the period of cotton lint harvesting, dissecting the mechanism of cotton defoliation using a highly accurate and comprehensive research technique is an unprecedented challenge. snRNA-seq enables independent transcriptomic analysis of individual cells, revealing functional and gene expression differences among different cell types and identifying dynamic cellular subpopulations involved in specific physiological processes. Compared to traditional tissue-level approaches, snRNA-seq is more suitable for revealing fine regulatory mechanisms. We found that during this response to defoliant, the cells in the AZ of cotton petioles gradually aged, and the degree of cell wall rigidity increased. The

application of snRNA-seq preserves cell integrity and vitality to some extent, thereby improving the quality and reliability of sequencing data and allowing us to obtain more comprehensive cellular transcriptomic information and better understand cellular functions and regulatory mechanisms. In our study, we employed snRNA-seq technology to construct a transcriptomic atlas of cotton petioles, identifying two cell types closely associated with petiole abscission: abscission cells (gene cluster 14) and protective layer cells (gene clusters 15 and 16) (**Supplemental Figure 2**). This was demonstrated by our identification of *GhRLF1* as a determinant of cell fate in abscission cells (cluster 14) and of important transcription factors involved in the transcriptional regulation of this gene (**Figure 2C**).

Cytokinins are known to delay leaf senescence and enhance the economic value of crops (Chen et al., 2020a; Zeng *et al.*, 2022; Zhang et al., 2021), but their role in leaf abscission is still being explored. In postharvest Chinese flowering cabbage, the transcriptional activator *BrNAC029* was shown to bind to the promoter of the cytokinin oxidase gene *BrCKX1*, activating its expression and reducing endogenous cytokinin levels, thus accelerating leaf senescence (Li et al., 2023). In our study, we discovered that the marker gene of the abscission cell cluster, *GhRLF1*, which is involved in the cytokinin degradation pathway, was continuously upregulated after chemical defoliant treatment until the petiole abscission period (**Figure 3H and Figure 5A**). This upregulation led to a decrease in endogenous cytokinin levels in the AZ (**Figure 3I and Supplemental Figure 6A**). To further investigate this decrease, we expressed *GhRLF1* in vitro and tested various common cytokinins as enzyme substrates (**Figures 3JG and 3K and Supplemental Figures 6B and 6C**). The results confirmed that the decrease in endogenous cytokinin levels is likely due to the irreversible degradation of *GhRLF1*, which disrupts cytokinin homeostasis in the AZ and contributes to cotton petiole abscission. Interestingly, we observed a difference in the expression level of *GhRLF1* between the residual AZ tissue on the main body (residuum cells) and the separated AZ tissue (secession cells) during the petiole abscission process (**Supplemental Figure 13**). Simultaneously, following defoliant induction, *GhRLF1* expression levels varied among the distal end (adjacent to the leaf apex), proximal end (middle portion of the petiole), and AZ, with the distal end seemingly maintaining a relatively high level (**Supplemental Figure 13**). This disparity is likely a consequence of the signal initiation and subsequent transmission triggered by leaf exposure to the defoliant, which warrants further exploration. Additionally, our study revealed that two transcription factors, GhWRKY70 and GhMYB108, are expressed in the AZ of cotton petioles and are upregulated by defoliants (**Figure 4A and Figure 5A**). Specifically, *GhWRKY70* and *GhMYB108* also exhibit higher expression levels at the distal axial end (**Supplemental Figure 13**). These transcription factors may play a role in regulating *GhRLF1* and enhancing sensitivity to chemical defoliants.

WRKY transcription factors have been shown in previous studies to be closely

associated with hormone signaling, the stress response, organ senescence, and abscission (Chen and Huang, 2022; Liu et al., 2023a). In the present study, GhWRKY70 was found to activate *GhRLF1* transcription by directly binding to the W-box element in the *GhRLF1* promoter (**Figures 4D-G**). A similar regulatory module, *SlWRKY17-SlIDL6*, has been identified in tomato, where it promotes floral organ abscission by increasing the expression of proteins involved in cell wall remodeling under low-light induction (Li et al., 2021). Furthermore, the phenotype of the *GhWRKY70* knockout mutant closely resembled that of the *GhRLF1* knockout mutant (**Figures 3D-Fand Figures 4H and 4I**). Therefore, we propose that under the influence of chemical defoliants as external stimuli, the *GhWRKY70-GhRLF1* regulatory module is triggered to induce petiole detachment (**Figure 7**). This process ultimately leads to the residuum cells showing a mostly rounded state, while the aging of the vascular bundle region structure results in a fractured state (**Figure 3E and Figure 7**). However, interestingly, defoliant treatment caused a sharp downregulation of *GhWRKY70* expression after 72 hours (**Figure 5A**). We speculate that this difference may be due to the regulation of *GhRLF1* transcription by GhWRKY70 in a cytokinin concentration-dependent manner. As the abscission process progresses, the GhRLF1 protein gradually accumulates and accelerates cytokinin degradation (**Figure 3I and Supplemental Figure 6A**). This leads to a decrease in endogenous cytokinin levels in the AZ, where cytokinin levels are insufficient for maintaining homeostasis. This triggers negative feedback regulation and results in a decrease in the expression level of *GhWRKY70* (Supplemental Figures 7A-D). The dose-dependent transcriptional regulation of this transcription factor has emerged as a determining factor for cell fate transition (Reddy and Meyerowitz, 2005; Wang and Zhang, 2017; Zhou et al., 2018). GhWRKY70 was shown to act as the "*Pioneer*" for the first half of the process, while the sustained high expression of *GhRLF1* prompted us to identify the "*Successor*" that maintains expression. After 48 hours of defoliant induction, *GhMYB108* exhibited an increase in expression; this gene can be considered the "*Successor*" in the second half of the abscission event, during which the transcriptional activation of *GhRLF1* was completed (**Figure 5A**). As the event progresses, the residuum cells will also exhibit rounded vascular bundle cells caused by natural shedding, as well as wrinkled cells that were previously exposed to air (**Figure7**).

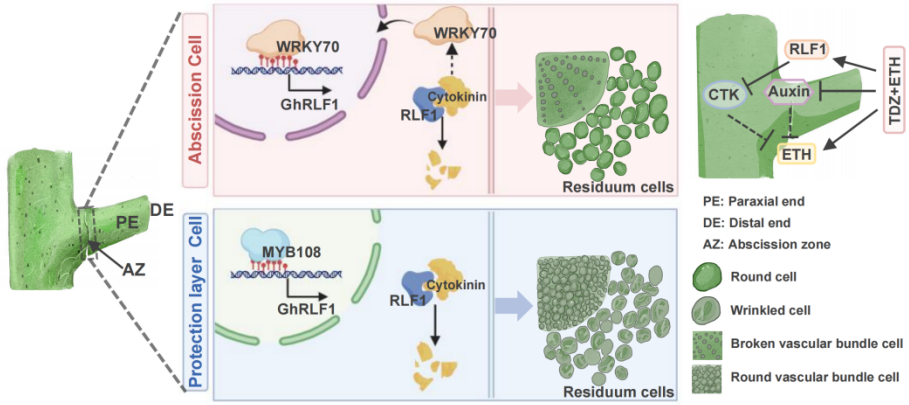

Figure 7 A schematic model of the chemical defoliation-related mechanism of the GhWRKY70/GhMYB108-*GhRLF1* module.

GhRLF1, an essential factor determining the fate of petiole AZ cell clusters, plays a positive regulatory role in entire process of cotton chemical defoliation. Temporally, GhWRKY70 and GhMYB108 synergistically activate the expression of *GhRLF1* in a stepwise manner, acting as the "*Pioneer*" and "*Successor*" respectively, to assist in the chemical defoliation of mechanically harvested cotton. Spatially, GhWRKY70 and GhMYB108 assume dominant roles in abscission cells and protection layer cells, respectively. In the interweaving process of time and space, the signals of plant hormones interfere with each other and jointly regulate the cell state of the petiole AZ.

GhRLF1 has the potential to enhance defoliation traits, and cytokinins play a crucial role in yield traits. The cytokinin oxidase/dehydrogenase coding gene, which controls CK levels, has been identified as a major quantitative trait locus (QTL) affecting rice grain number (Zhang et al., 2012). However, in our study, GUS staining revealed strong expression driven by both the strong promoter *pro35S* and *proGhRLF1* in the AZ and ovule (**Supplemental Figure 11C**). This resulted in the overexpression of *GhRLF1*, which led to an increased defoliation rate and decreased cytokinin content in the ovule, directly impacting yield (**Figure 3G and Figure 6C and Supplemental Figure 6A**). Therefore, finding a balance between defoliation effects and yield is of utmost importance. *AtPER21*, a member of the peroxidase family, was identified as an upregulated gene in the Arabidopsis stamen AZ. It acts as a regulatory factor for cell wall modification proteins and hormone metabolism pathways during abscission (Cai and Lashbrook, 2008). In the present study, we showed that *GhPER21* is expressed predominantly in the AZ, with minimal expression in the ovule, and its expression is upregulated by defoliant treatment (**Supplemental Figures 11C and 11D**). In contrast to the other genes studied, *GhPER21* exhibited a more pronounced and specific

expression pattern in the proximal axial end and AZ, which may be closely associated with its crucial role (**Supplemental Figure 13**). The *proPER21::RLF1* overexpression lines not only exhibited increased sensitivity to defoliants but also exhibited stable yield traits (**Figure 6H and Supplemental Figure 11E**). Therefore, while manipulating *GhRLF1* to increase defoliation, ensuring that gene expression occurs in appropriate tissues is crucial. Even more excitingly, overexpression of *GhRLF1* can enhance the sensitivity of cotton leaves to defoliants, resulting in a 30% reduction in the dosage of chemical defoliants while achieving the same level as the wild type (**Supplemental Figures 12A-C**). This discovery contributes to both economic and environmental benefits, providing strong reference for breeding.

In numerous previous research reports on the precise abscission of plant organs, greater attention has been paid to ethylene, auxin, and peptide signal pathways such as receptor-like kinases, while neglecting cytokinins, which promote cell division, plant tissue growth, and repair (文献). Our study confirms that the application of chemical defoliant induces the upregulation of the cytokinin oxidase gene *GhRLF1* in the abscission zone of petioles, irreversibly degrading cytokinins, disrupting hormone homeostasis, and leading to petiole abscission (**Figures 3G-I and Supplemental Figure 5A**). Plant development accompanies carbon resource consumption, leading to organ abscission due to competition for assimilates, and the auxin signaling protein RhARF7 positively regulates the expression of the sucrose transporter protein SUC2 (文献). Low light induces a peptide, CLV3, which regulates the fate of meristematic stem cells, and suppresses the expression of SLWUS. Through disrupting the response gradient of auxin concentration and ethylene production, it eventually leads to flower organ abscission ((Cheng *et al.*, 2022)). The IDA-HAE/HSL2 signaling pathway and the NEV-CST/EVR signaling pathway have been extensively investigated in the abscission process of flower organs in Arabidopsis ((Burr et al., 2011; Shi *et al.*, 2011)). Our study also revealed that genes related to the ethylene and auxin pathways might respond to chemical defoliants in opposite manners(**Supplemental Figure 4C**); moreover, the ethylene signaling pathway, the abscisic acid and auxin signaling pathways, the IDA and NEV signaling pathways, and previously reported genes related to organ abscission might all have crosstalk with the cytokinin pathway, especially the response factors related to ethylene signal transduction, the ethylene biosynthesis pathway, and the abscisic acid pathway (**Supplemental Figure 13 and Supplemental Figure 14 and Supplemental Figure 15**). The majority of these pathway genes were not detected in the Top 50 of each cluster in the snRNA-seq data, especially the IDA and NEV pathways (**Supplemental Table 3**). Nevertheless, these classical organ abscission pathways still merit further in-depth exploration.

This work demonstrates that by manipulating to increase the expression of *GhRLF1* in the abscission zone of cotton petioles and thereby reducing the endogenous cytokinin content, it provides a biotechnological solution for enhancing the sensitivity of crops to chemical defoliants, with potentially significant benefits for mechanical harvesting of cotton, reducing chemical inputs in agriculture and stabilizing production to increase income for farmers.

METHODS

Plant materials, growth conditions and defoliant treatments

The wild-type cotton materials used in this study were Jin668 and Xinluzao50 (X50) (*Gossypium hirsutum*), which were cultivated in a cotton greenhouse at Huazhong Agricultural University in Wuhan, China, along with the transgenic materials. The light cycle was set to 14 hours of light and 10 hours of darkness, while the temperature was maintained between 28°C and 32°C. Proper water and fertilizer management were implemented. Additionally, all cotton materials were planted in the experimental field of Huazhong Agricultural University and managed appropriately. Tobacco (*N. benthamiana*) was grown in the auxiliary building of the greenhouse at Huazhong Agricultural University with a light cycle of 12 hours of light and 12 hours of darkness. The temperature was maintained between 25°C and 28°C, and Hoagland nutrient solution was used for irrigation. The growth cycle of the tobacco plants was approximately 4 weeks.

The chemical defoliant used in this study was XinSaiLi (10% thidiazuron + 40% ethephon + auxiliary agent), and the working solution was prepared at a concentration of 1‰. The plants were sprayed under stable temperature conditions, ensuring that the average temperature throughout the day was not less than 12°C. It was important to avoid spraying plants under strong light conditions. If rainfall occurred within 12 hours after spraying, supplementary spraying was needed. The effective period for defoliant spraying was 7 days, with a critical period of 3 days.

Single-cell nucleus suspension preparation and snRNA-seq library construction

Abscission zone (AZ) was placed on a glass plate with 300 μl of Nuclei Isolation Buffer (NIB, 20 mM HEPES (pH 8.0), 250 mM sucrose, 1 mM $MgCl_2$, 5 mM KCl, 40% glycerol, 0.25% Triton, 0.1 mM PMSF, 0.1% β-Me, 0.2 U/μl Protector RNase Inhibitor). Next, the samples were chopped with a sterile razor blade for 5 minutes. The homogenate was transferred from the glass plate to a 2 ml centrifuge tube and incubated on a rocking shaker for 5 minutes with gentle horizontal shaking. Next, the samples were filtered through a 100 μm strainer placed on top of a 2 ml centrifuge tube placed on ice. Centrifugation at 10,000 ×g for 2 minutes at 4°C was applied to collect the nuclei at the bottom of the tube. After centrifugation, the supernatant was carefully removed, and the pellet was resuspended in 350 μl of NIB Wash

(50 mM Tris-HCl (pH 7.9), 100 mM NaCl, 10 mM $MgCl_2$, 1 mM DTT, and 0.2 U/μl Protector RNase Inhibitor). The nuclei and cell debris were then separated using a 20 μm strainer. Nuclei were stained with DAPI solution for flow cytometric sorting using a BD FACS cell sorter. Sorted nuclei were collected together as one replicate of a sample. A final resuspension that enables a concentration of approximately 400-700 nuclei/μl after sorting was found to be optimal. The nuclear suspension was kept on ice throughout the procedure to prevent RNA degradation.

The snRNA-seq libraries were constructed using the Chromium Next GEM Single Cell 3′ GEM, Library & Gel Bead Kit v3.1 following the user manual provided with the kit. The libraries were sequenced on an Illumina sequencing platform using the BGI PE100 strategy.

Nucleus clustering and reconstruction of cell trajectories by nonlinear dimensionality reduction

The original snRNA-Seq dataset was aligned with the TM-1 genome, and Cell Ranger (version 6.1.1; 10X Genomics) was used to analyze and generate the cell expression matrix. Subsequently, the cell expression matrix was analyzed using the Seurat package in the R environment. To ensure the accuracy and reliability of the data, we filtered out cells with gene sequence counts less than 1000 or greater than 20000 and fewer than 500 or more than 8000 gene features, as well as cells with mitochondrial and chloroplast sequence percentages exceeding 0.8% and low-quality cells expressing fewer than three genes, which could occur due to low sequencing depth, low gene expression, or high noise levels. The filtered dataset was then batch-corrected using the Harmony package and standardized and normalized using the “ScaleData” and “NormalizeData” functions to reduce technical differences between cells and samples. The top 3000 highly variable genes were subjected to principal component analysis (PCA) to reduce dimensionality, and a resolution of "0.2" was used with the FindClusters function to identify cell clusters. The data structures and cell trajectories were visualized and explored using t-SNE and UMAP. To determine the cell types in each cluster, we performed enrichment analysis of the gene markers using the FindMarkers function provided by Seurat. Differential expression analysis was conducted using the Wilcoxon rank-sum test. The cluster-enriched genes were detected using the parameters min.pct = 0.5 and min.diff.pct = 0.3.

Pseudotime analysis

To reconstruct the cellular changes over time, we used the Monocle2 package to construct cell trajectories. The “newCellDataSet” function in Monocle was used to convert the single-cell expression matrix into the desired data format. Then, we preprocessed the data, including by gene filtering and normalization, using the “preprocessCDS” function in Monocle. Next, we

used the “reduceDimension” function in Monocle to perform dimensionality reduction to capture the major variations between cells. The “orderCells” function with max_components = 2 and method = 'DDRTree' was used to construct a pseudotime series, and the trajectory plot was generated using plot_cell_trajectory.

RNA in situ hybridization

In this study, gene-specific probes were prepared according to the manual of the DIG Northern Starter Kit (Roche). The probes obtained were dissolved in 50% (v/v) deionized formamide and stored at -80°C until use. In situ hybridization was performed following previously established methods in cotton research (Zhang et al., 2017). Abscission zone collected 48 hours after defoliant treatment were embedded in paraffin. Paraffin sections (10 μm thick) were deparaffinized, rehydrated, and incubated overnight with a Dig-labeled RNA probe (Roche). Subsequently, the sections were incubated with alkaline phosphatase-conjugated anti-digoxigenin (anti-Dig-AP; Roche), and the signal was detected using nitro-blue tetrazolium/5-bromo-4-chloro-3-indolyl-phosphate (NBT/BCIP) color substrate solution (Roche). Sections incubated with the sense RNA probe served as the negative control. Images were captured using a fully motorized upright fluorescence microscope (Leica DM6B) in bright-field mode. The primers used are listed in **Supplemental Table 5**.

Candidate gene association analysis and linkage disequilibrium

A total of 4,098,410 high-quality SNP loci were obtained after genotype filtering of 517 cotton accessions (MAF≥5%, missing rate ≤5%). The mixed linear model in FastLMM (Factored Spectrally Transformed Linear Mixed Models) software was utilized, with the PCA clustering results serving as covariates for GWAS. The number of effective SNP loci (1,044,240.44) was calculated using the Genetic Type I error calculator (GEC) software, and the significance threshold for the 517 natural populations was 9.58×10^{-7}.

The position structure of the gene was obtained based on the reference genome, and the P-value corresponding to the SNP within the gene interval was extracted from the genome-wide association analysis result file. LDBlockShow software was employed along with the genotype file and reference genome to generate local Manhattan plots and LD heat maps. Missense SNP variation information within the gene interval was extracted and combined with phenotype data, and violin plots of different haplotypes were created using R.

RNA extraction and quantitative real-time PCR (RT–qPCR)

We used the HiPure HP Plant RNA Mini Kit (Magen) for RNA extraction from plant tissue samples. Approximately 2.5 μg of high-quality RNA was reverse transcribed into cDNA using

the HiScript®II 1st Strand cDNA Synthesis Kit (Vazyme), and the obtained cDNA was diluted 100-fold to create the working solution. Real-time quantitative PCR assays were performed on a QuantStudio 6 Flex (Thermo Fisher) using ChamQ SYBR Color qPCR Master Mix (Vazyme). *GhUbiquitin* (*GhUB7*) was used as the internal reference for RT–qPCR, and the specific primer sequences can be found in **Supplemental Table 5**. For RT–qPCR experiments, at least 3 biological replicates were performed.

Gene cloning, vector construction and genetic transformation

By using specific primers, the full-length transcript sequences of *GhRLF1* and *GhMYB108* were amplified. These sequences were subsequently cloned and inserted into the pDONR/Zeo vector. *GhRLF1* was subsequently inserted into the pK2GW7 overexpression vector with CaMV35S as the promoter to generate the *35S::GhRLF1* recombinant plasmid. *GhMYB108* was subsequently inserted into the pGWB451 vector to generate the recombinant GhMYB108-GFP overexpression plasmid.

The same method was used to amplify approximately 1.5 kb from the start codon ATG of *GhRLF1* and *GhPER21* from the genome. These sequences were subsequently cleaved into pKGWFS7 vectors harboring EGFP and GUS sequence elements to obtain the *proRLF1::GFP-GUS* and *proPER21::GFP-GUS* vector plasmids, respectively.

The *proPER21::RLF1* vector was generated by replacing the 35S sequence with the *GhPER21* promoter sequence based on the *35S::GhRLF1* vector. All the mutant vector plasmids were created using the clustered regularly interspaced short palindromic repeats (CRISPR)/CRISPR associated nuclease 9 (Cas9) system (Wang et al., 2018).

All the abovementioned vector plasmids were introduced into Agrobacterium strain GV3101 through electric shock transformation. Transgenic lines were obtained by transforming cotton Jin668 according to previously reported methods (Karimi et al., 2002; Wang *et al.*, 2018). All primers used for vector construction are detailed in **Supplemental Table 5**.

Observation of histological sections, cytology scanning electron microscopy, GFP fluorescence, and histochemical staining of β-glucuronidase activity

The tissue in the AZ was sampled and fixed, followed by embedding in paraffin. Then, a paraffin slicer (Leica, Thermo) was used to longitudinally slice the AZ. After staining with toluidine blue, the formation of fracture zones was observed under a stereomicroscope (Nikon).

A safety blade was used to cut and remove approximately 3 mm of detached tissue that remained on the main body after manually removing the cotton petiole. The removed tissue was then fixed in 2.5% glutaraldehyde. After vacuum drying and sputter coating, the cell state

of the fractured plane was observed using a scanning electron microscope (JSM-6390/LV).

During the hydroponic seedling stage of plants, the tissue parts that need to be observed are sliced by hand. Then, under a confocal microscope (Olympus FV1200), the laser emission peak is 488nm, and GFP fluorescence is observed.

After sampling the plant tissue, the plants were immersed in a 1 mg/ml X-β-D-glucuronide (X-Gluc, GUS, Yeasen) staining solution in the dark and incubated overnight at 37°C until a clear blue color appeared. The tissue was stained with 75% ethanol until the negative control material turned white. Then, the stained tissue was observed under a stereomicroscope. Additionally, the GUS staining spots were very stable and did not fade in ethanol.

Determination of endogenous cytokinins and detection of in vitro enzyme activity

Fresh tissue samples from the cotton petiole AZ were ground in liquid nitrogen. Briefly, 0.05 g of fresh plant sample was mixed with 10 μl of an internal standard solution at a concentration of 100 ng/ml. Then, 1 ml of an extraction agent consisting of methanol/water/formic acid (15:4:1, v/v/v) was added. The samples were vigorously vortexed for 10 minutes, after which the supernatant was concentrated and redissolved in 100 μl of an 80% methanol/water solution. The samples were filtered through a 0.22 μm membrane for LC–MS/MS analysis. The main data collection techniques used were ultraperformance liquid chromatography (UPLC, ExionLC™ AD) and tandem mass spectrometry (MS/MS, QTRAP®6500+). Both the chromatographic and mass spectrometry methods were used according to previously described methods (Cui et al., 2015; Xiao et al., 2018). Three biological replicates were performed for each sample.

The full-length CDS of *GhRLF1* was cloned and inserted into the pGEX-4T-1 vector, after which overexpression of the GST-tagged protein was induced in *Escherichia coli BL21* (DE3) cells. Protein purification was performed using a glutathione S-transferase column (Pierce Glutathione Agarose, Thermo). Then, following previously described methods(Zhang *et al.*, 2021), five cytokinins (Yuanye Bio-Technology or Sigma), namely, zeatin (CZ), trans-zeatin (tCZ), DL-dihydrozeatin (DHZ), N6-(delta2-isopentenyl)-adenine (2-IP), and trans-zeatin-riboside (tZR), were used as substrates and incubated with purified proteins at 37°C overnight. After the reaction was completed, the supernatant was filtered through a 0.22 μm membrane for high-performance liquid chromatography (HPLC) analysis.

Y1H, LUC and electrophoretic mobility shift assay (EMSA)

The entire cDNA sequence of *GhMYB108* was cloned and inserted into the pGADT7 vector, and each truncated promoter generated by deleting a binding site starting from the 5′-end according to the positions of the MYB binding sites was cloned and inserted into the pAbAi

vector. After linearization, the resulting sequence was integrated into the Y1HGold yeast genome. The recombinant vector *pGADT7-GhMYB108* and the empty vector pGADT7 were subsequently transformed into the Y1HGold yeast strain, which contains the inducible sequence fragment. Screening of the appropriate concentration of aureobasidin A (AbA, Takara) was performed according to the manufacturer's instructions.

The dual-luciferase (LUC) reporter assay was conducted as previously described (Hu et al., 2018). The full-length coding sequences of *GhWRKY70* and *GhMYB108* were cloned and inserted into the pGreenII 62-SK vector and used as effectors in the dual-luciferase reporter assay system. The *GhRLF1* promoter sequence was truncated by deleting a binding site starting from the 5′-end according to the positions of the W-box and MYB binding sites. The truncated promoter sequences were subsequently inserted into pGreenII 0800-LUC vectors to stimulate the expression of firefly luciferase (LUC) reporters. The reporters and effectors were coinfiltrated into tobacco leaves via Agrobacterium, and the growth cycle was approximately 4 weeks. After 60 to 72 hours, LUC luminescence was detected using a cryogenically cooled CCD camera (Berthold). Empty pGreenII 62-SK was used as a negative control. The experiment had at least three biological replicates. The primers used for the LUC experiments are detailed in **Supplemental Table 5**.

For determination of LUC activity in cotton protoplasts, 40% polyethylene glycol 4000 (PEG 4000, Sigma) was used to mediate the transfer of genetic factors into recipient cell protoplasts. The effectors and reporters were cotransformed into cotton protoplasts under certain concentrations of CaCl2 (Sigma) and PEG. The mixture was incubated overnight at 25°C-28°C in the dark, after which the activities of firefly luciferase and Renilla luciferase were measured using dual-luciferase reporter assay reagents (Promega, Madison, WI, USA), and the LUC/REN ratio was analyzed. At least three biological replicates were performed for each sample.

The full-length coding sequences of *GhWRKY70* and *GhMYB108* were fused with GST tags and subsequently cloned and inserted into the pGEX-4T-1 vector (Invitrogen). The proteins expressed in *Escherichia coli BL21* (DE3) were purified using the MagneGST Protein Purification System (Cat. #V8600, Promega). Biotin-labeled single-stranded DNA was synthesized and annealed to form double-stranded DNA. The combination reaction was carried out using the LightShift Chemiluminescent EMSA Kit (Thermo Scientific, 20148) following the manufacturer's instructions. A GST antibody (Abclonal) was used to bind the protein and DNA binding complexes. A quantitative western blot imaging system (Tanon) was used for imaging. The primers used for vector construction are shown in **Supplemental Table 5**.

DATA AVAILABILITY

The clean raw sequencing data of snRNA-seq data have been deposited in NCBI database under accession number PRJNA1014698. All other data are included in the manuscript.

FUNDING

This work was supported by funding from the National Key Project of Research and the Development Plan of China (2021YFF1000103), National Natural Science Foundation of China (no. 32171942), The development fund for Xinjiang talents XL, and Agricultural GG Project of Xinjiang Production and Construction Corps (NYHXGG, 2023AA102).

AUTHOR CONTRIBUTIONS

XY and XZ designed and guided the project. KL, LZ, MW, HX and YY gave comments on the project. BZ and DY performed experiments and wrote the manuscript. BH and DB performed bioinformatic analyses. XZ, XH and XL provided intellectual input. XY and XZ revised the manuscript. All authors read and/or edited the manuscript.

ACKNOWLEDGMENTS

The computations in this paper were run on the bioinformatics computing platform of the National Key Laboratory of Crop Genetic Improvement, Huazhong Agricultural University.

COMPETING INTERESTS

These authors declare no competing interests.

SUPPLEMENTAL INFORMATION

Supplemental Figure 1 Correlation between two biological replicates of snRNA-Seq.

The PCA (A) and UMAP visualization (B) shows cells in cotton petioles at 0, 3, 6, 12, 24 and 48 hours after defoliant treatment. The horizontal and vertical coordinates are two principal components, and the dots represent different cells, in which different colors represent different replicates.

Supplemental Figure 2 Visualization of cell clusters in abscission zone of cotton petioles and marker genes in each cell clusters.

t-SNE visualization of 14 cell clusters (0-13) in X50_0 (before treatment) (A) and 14 cell clusters (0-9, 11, 14-16) in X50_All (before and after treatment) (B) Different colors represent different cell clusters, as in Figure 2. (C) UMAP visualization shows the emergence of abscission cells and protective layer cells in cotton petiole after different time points of defoliant treatment. Different numbers and colors represent different cell clusters, as in Figure 2. (D) Heatmap of top 5 genes enriched in each cell cluster in X50_0. Color bar indicates the scaled expression level. (E) Expression of top 5 genes enriched in each cell cluster in X50_0. Color, mean expression across cells in that cluster; dot diameter, proportion of cluster cells expressing a given gene. (F) Heatmap of top 5 genes enriched in each cell cluster in X50_All. (G) Expression of top 5 genes enriched in each cell cluster in X50_All.

Supplemental Figure 3 GO enrichment analysis of the DEGs of different cell clusters in cotton.

(A) GO enrichment analysis of abscission cells (cluster 14). (B) GO enrichment analysis of protective layer cells (cluster 16). (C) GO enrichment analysis result of the DEGs of different clusters.

Supplemental Figure 4 Hierarchical cluster tree of abscission cells showing co-expression modules identified by hdWGCNA.

(A) Gene module classification of abscission cells. Each leaf in the tree is one gene. The major tree branches constitute several gene modules labeled by different colors. Red triangles point to the module (blue) containing genes enriched in abscission cluster. (B) Co-expression network of core genes related to the initiation of abscission. Lines indicate edge weight for each pair of genes. Each circle represents a gene. (C) Analysis of the expression patterns of selected genes associated with auxin and ethylene signaling at different time points before and after treatment with the chemical defoliant.

Supplemental Figure 5 Measurement of endogenous cytokinin content in the abscission zone of cotton petioles and in vitro enzyme activity of GhRLF1 protein.

(A)Measurement of endogenous cytokinin content in the abscission zone of cotton petioles in the wild-type and *GhRLF1* overexpression lines at various time points following chemical defoliant spraying. N6-(delta 2-isopentenyl)-adenine (IP), N6-isopentenyladenosine (IPR), kinetin-9-glucoside (K9G), cis-zeatin (cZ), trans-zeatin (tZ), trans-zeatin riboside (tZR). The values in (A) are the means ± SEs (n = 3). (B and C) High-performance liquid chromatography (HPLC) diagrams showing the degradation of cytokinins by GhRLF1 protein expressed in vitro. The amount of cytokinin used in the experimental group remained consistent. Adenine (Ade) was used as a product standard and serves as a positive control.

Supplemental Figure 6 Determination of editing efficiency and paraffin section image of *GhWRKY70* transgenic lines

(A) Detection of editing efficiency for wrky70#1/2. (B) The longitudinal images of the petiole abscission zone in the wild-type and *GhWRKY70* knockout mutants at different time points after defoliant treatment, respectively. Bars = 100μm.

Supplemental Figure 7 Cytokinin induces elevated transcriptional levels of *GhWRKY70*.

(A) Immunoblots showing WRKY70 protein levels after cytokinin analog (6-BA) treated alone, and with protein synthesis inhibitor CHX (Cycloheximide) together. 35S:WRKY70-GFP construct was transformed into cotton protoplast cells for 12 h and then treated with 1μM CHX for 2 h, or not, before being treated with 1μM 6-BA. Rubisco protein was used as control. (B) Relative intensities of protein bands in (A). Data obtained using ImageJ software. The data was means ± SEs (n = 3). (C) RT-qPCR results of each group of samples in (A). The values were determined by RT-qPCR and were means ± SEs (n >= 3). *GhUB7* was used as internal reference. (D) Relative expression levels of *GhWRKY70* in the petiole abscission zones of *rlf1* and *35S::RLF1* transgenic lines were detected by RT-qPCR, revealing differences compared to the wild type. The values were determined by RT-qPCR and were means ± SEs (n = 4). *GhUB7* was used as internal reference.

Supplemental Figure 8 Enrichment and expression patterns of GhRLF1 and GhMYB108.

Enrichment and expression patterns of *GhRLF1* and *GhMYB108* in various cell clusters at different time points following defoliant treatment.

Supplemental Figure 9 GhMYB108 has the ability to bind to the MYB-binding site on *GhRLF1* promoter.

Transient dual-luciferase reporter assays in tobacco leaves. The bioluminescence intensity and numerical value reflect the strength of the binding of GhMYB108 to the *GhRLF1* promoter. EV indicates the empty pGreenII 62-SK vector, which was used as a control. The values were means ± SEs (n >= 6 leaves).

Supplemental Figure 10 Determination of editing efficiency and paraffin section image of *GhSMYB108* transgenic lines

(A) Detection of editing efficiency for myb108#*6* and myb108#*7*. (B) The longitudinal images of the petiole abscission zone in the wild-type and GhMYB108 transgenic lines after 48 and 72 hours of defoliant treatment, respectively. Bars = 100μm.

Supplemental Figure 11 Analysis of tissue expression patterns of GhRLF1 and GhPER21.

(A) GFP fluorescence of *pro35S:: GFP-GUS* and *proRLF1:: GFP-GUS*. Bars = 20μm. (B) GFP fluorescence of *proPER21:: GFP-GUS*. Bars = 20μm. (C) GUS staining of *pro35S::GFP-GUS* , pro*RLF1::GFP-GUS* and *proPER21::GFP-GUS* transgenic cotton lines. The tissues include stem, leaf, stigma, ovule, anther and petiole. Bars = 1000μm. (D) Expression patterns of *GhPER21* in various cotton tissues. The values were determined by RT-qPCR and were means ± SEs (n = 3). *GhUB7* was used as internal reference. (E) Comparison of cotton bolls size at 5 DPA, 10 DPA, 15 DPA between wild-type and *proPER21::RLF1* transgenic lines. Bars = 1cm.

Supplemental Figure 12 Field performance of *GhRLF1* related transgenic lines.

(A and B) Field phenotypes of *GhRLF1* related transgenic lines in Xinjiang before and 7 days after 100% and 70% defoliant treatment, respectively. (C) Statistics of defoliation rate of all experimental groups in (A) before and after defoliant treatment on the 5th, 6th and 7th day. The values in (C) are the means ± SEs (n >= 5).

Supplemental Figure 13 Analysis of the expression patterns of the studied genes in tissues related to the abscission zone.

After defoliant treatment, the expression patterns of *GhRLF1*, *GhWRKY70*, *GhMYB108* and *GhPER21* in residuum cells, secession cells, distal end, middle petiole (Paraxial end), and abscission zone were observed. The values were determined using RT-qPCR and presented as means ± SEs (n = 3). *GhUB7* was used as an internal reference.

Supplemental Figure 14 Analysis of gene expression patterns related to hormone signaling pathway and peptide signaling pathway.

Expression patterns of related genes in hormone signaling pathway and peptide signaling pathway in *GhRLF1* transgenic lines and wild-type before and 48h after defoliant treatment. The values were determined using RT-qPCR and presented as means ± SEs (n = 3). *GhUB7* was used as an internal reference.

Supplemental Figure 15 Analysis of reported gene expression patterns associated with plant organ abscission.

Expression patterns of reported gene expression patterns associated with plant organ abscission in *GhRLF1* transgenic lines and wild-type before and 48h after defoliant treatment. The values were determined using RT-qPCR and presented as means ± SEs (n = 3). *GhUB7* was used as an internal reference.

Supplemental information

Supplemental Table1: Summary statistics of snRNA-seq data.

Supplemental Table 2: Marker genes of each cell cluster in X50_0.

Supplemental Table 3: Marker genes of each cell cluster in X50_All.

Supplemental Table 4: Marker genes of each sub-cell clusters of petiole abscission cells

Supplemental Table 5: Primers used in this study.

REFERENCES

Burr, C.A., Leslie, M.E., Orlowski, S.K., Chen, I., Wright, C.E., Daniels, M.J., and Liljegren, S.J. (2011). CAST AWAY, a Membrane-Associated Receptor-Like Kinase, Inhibits Organ Abscission in Arabidopsis. Plant Physiol. **156**:1837-1850. 10.1104/pp.111.175224.

Cai, S.Q., and Lashbrook, C.C. (2008). Stamen abscission zone transcriptome profiling reveals new candidates for abscission control: Enhanced retention of floral organs in Transgenic plants overexpressing Arabidopsis ZINC FINGER PROTEIN2. Plant Physiol. **146**:1305-1321. 10.1104/pp.107.110908.

Chakrabarti, M., and Bharti, S. (2023). Role of EIN2-mediated ethylene signaling in regulating petal senescence, abscission, reproductive development, and hormonal crosstalk in tobacco. Plant Sci. **332**:11. 10.1016/j.plantsci.2023.111699.

Chang, H.S., Jones, M.L., Banowetz, G.M., and Clark, D.G. (2003). Overproduction of cytokinins in petunia flowers transformed with P(SAG12)-IPT delays corolla senescence and decreases sensitivity to ethylene. Plant Physiol. **132**:2174-2183. 10.1104/pp.103.023945.

Chen, L., Zhao, J.Q., Song, J.C., and Jameson, P.E. (2020a). Cytokinin dehydrogenase: a genetic target for yield improvement in wheat. Plant Biotechnol. J. **18**:614-630. 10.1111/pbi.13305.

Chen, N.C., Wang, H., Abdelmageed, H., Veerappan, V., Tadege, M., and Allen, R.D. (2020b). HSI2/VAL1 and HSL1/VAL2 function redundantly to repress DOG1 expression in Arabidopsis seeds and seedlings. New Phytol. **227**:840-856. 10.1111/nph.16559.

Chen, W., and Huang, B.R. (2022). Cytokinin or ethylene regulation of heat-induced leaf senescence involving transcriptional modulation of WRKY in perennial ryegrass. Physiol. Plantarum. **174**:10. 10.1111/ppl.13766.

Chen, Y., Tong, S.F., Jiang, Y.Z., Ai, F.D., Feng, Y.L., Zhang, J.L., Gong, J., Qin, J.J., Zhang, Y.Y., Zhu, Y.Y., et al. (2021). Transcriptional landscape of highly lignified poplar stems at single-cell resolution. Genome Biol. **22**:22. 10.1186/s13059-021-02537-2.

Cheng, L.N., Li, R.Z., Wang, X.Y., Ge, S.Q., Wang, S., Liu, X.F., He, J., Jiang, C.Z., Qi, M.F., Xu, T., et al. (2022). A SlCLV3-SlWUS module regulates auxin and ethylene homeostasis in low light-induced tomato flower abscission. Plant Cell **34**:4388-4408. 10.1093/plcell/koac254.

Chi, Y.J., Yang, Y., Zhou, Y., Zhou, J., Fan, B.F., Yu, J.Q., and Chen, Z.X. (2013). ProteinProtein interactions in the regulation of WRKY transcription factors. Mol. Plant. **6**:287-300. 10.1093/mp/sst026.

Cho, S.K., Larue, C.T., Chevalier, D., Wang, H.C., Jinn, T.L., Zhang, S.Q., and Walker, J.C. (2008). Regulation of floral organ abscission in Arabidopsis thaliana. Proc. Natl. Acad. Sci. U. S. A. **105**:15629-15634. 10.1073/pnas.0805539105.

Cui, K.Y., Lin, Y.Y., Zhou, X., Li, S.C., Liu, H., Zeng, F., Zhu, F., Ouyang, G.F., and Zeng, Z.X. (2015). Comparison of sample pretreatment methods for the determination of multiple phytohormones in plant samples by liquid chromatography-electrospray ionization-tandem mass spectrometry. Microchemical J. **121**:25-31. 10.1016/j.microc.2015.02.004.

Estornell, L.H., Agusti, J., Merelo, P., Talon, M., and Tadeo, F.R. (2013). Elucidating mechanisms underlying organ abscission. Plant Sci. **199**:48-60. 10.1016/j.plantsci.2012.10.008.

Farmer, A., Thibivilliers, S., Ryu, K.H., Schiefelbein, J., and Libault, M. (2021). Single-nucleus RNA and ATAC sequencing reveals the impact of chromatin accessibility on gene expression in Arabidopsis roots at the single-cell level. Mol. Plant. **14**:372-383. 10.1016/j.molp.2021.01.001.

Gala, H.P., Lanctot, A., Jean-Baptiste, K., Guiziou, S., Chu, J.C., Zemke, J.E., George, W.,

Queitsch, C., Cuperus, J.T., and Nemhauser, J.L. (2021). A single-cell view of the transcriptome during lateral root initiation in Arabidopsis thaliana. Plant Cell **33**:2197-2220. 10.1093/plcell/koab101.

Gao, S.P., Fang, J., Xu, F., Wang, W., Sun, X.H., Chu, J.F., Cai, B.D., Feng, Y.Q., and Chu, C.C. (2014). Cytokinin oxidase/dehydrogenase4 integrates cytokinin and auxin signaling to control rice crown root formation. Plant Physiol. **165**:1035-1046. 10.1104/pp.114.238584.

Geng, L., Li, Q., Jiao, L., Xiang, Y., Deng, Q., Zhou, D.-X., and Zhao, Y. (2022). WOX11 and CRL1 act synergistically to promote crown root development by maintaining cytokinin homeostasis in rice. New Phytol. **237**:204-206. 10.1111/nph.18522.

Graeff, M., Rana, S., Wendrich, J.R., Dorier, J., Eekhout, T., Fandino, A.C.A., Guex, N., Bassel, G.W., De Rybel, B., and Hardtke, C.S. (2021). A single-cell morpho-transcriptomic map of brassinosteroid action in the Arabidopsis root. Mol. Plant. **14**:1985-1999. 10.1016/j.molp.2021.07.021.

Habib, N., Li, Y.Q., Heidenreich, M., Swiech, L., Avraham-Davidi, I., Trombetta, J.J., Hession, C., Zhang, F., and Regev, A. (2016). Div-Seq: Single-nucleus RNA-Seq reveals dynamics of rare adult newborn neurons. Science **353**:925-928. 10.1126/science.aad7038.

Hönig, M., Plíhalová, L., Husicková, A., Nisler, J., and Dolezal, K. (2018). Role of Cytokinins in Senescence, Antioxidant Defence and Photosynthesis. Int. J. Mol. Sci. **19**:23. 10.3390/ijms19124045.

Hu, Q., Zhu, L.F., Zhang, X.N., Guan, Q.Q., Xiao, S.H., Min, L., and Zhang, X.L. (2018). GhCPK33 negatively regulates defense against verticillium dahliae by phosphorylating GhOPR3. Plant Physiol. **178**:876-889. 10.1104/pp.18.00737.

Huang, S.Z., Yamamoto, H., Ide, N., Mizuno, S., Shiraishi, N., Sato, T., Nakagawa, H., and Sonoda, M. (2010). Isolation and molecular characterization of a SoWRKY1 transcription factor from spinach (Spinacia oleracea). Plant Biotechnol. **27**:121-129. 10.5511/plantbiotechnology.27.121.

Jiang, C.Y., Liang, Y., Deng, S.N., Liu, Y., Zhao, H.H., Li, S.S., Jiang, C.Z., Gao, J.P., and Ma, C. (2023). The RhLOL1-RhILR3 module mediates cytokinin-induced petal abscission in rose. New Phytol. **237**:483-496. 10.1111/nph.18556.

Karimi, M., Inze, D., and Depicker, A. (2002). GATEWAY((TM)) vectors for Agrobacterium-mediated plant transformation. Trends Plant Sci. **7**:193-195. 10.1016/s1360-1385(02)02251-3.

Kim, J.Y., Symeonidi, E., Pang, T.Y., Denyer, T., Weidauer, D., Bezrutczyk, M., Miras, M., Zollner, N., Hartwig, T., Wudick, M.M., et al. (2021). Distinct identities of leaf phloem cells revealed by sin e cell transcriptomics. Plant Cell **33**:511-530. 10.1093/plcell/koaa060.

Lee, Y., Yoon, T.H., Lee, J., Jeon, S.Y., Lee, J.H., Lee, M.K., Chen, H.Z., Yun, J., Oh, S.Y., Wen, X.H., et al. (2018). A lignin molecular brace controls precision processing of cell walls critical for surface integrity in Arabidopsis. Cell **173**:1468-+. 10.1016/j.cell.2018.03.060.

Lewis, M.W., Leslie, M.E., and Liljegren, S.J. (2006). Plant separation: 50 ways to leave your mother. Curr. Opin. Plant Biol **9**:59-65. 10.1016/j.pbi.2005.11.009.

Li, F.J., Shan, Y.X., Wang, H.B., Jiang, G.X., Ding, X.C., Liang, H.Z., Wang, C.L., Kong, X.J., Xie, L.H., and Jiang, Y.M. (2023). A NAC transcriptional factor BrNAC029 is involved in cytokinin-delayed leaf senescence in postharvest Chinese flowering cabbage. Food Chem **404**:134657. 10.1016/j.foodchem.2022.134657.

Li, F.J., Wu, Q., Liao, B.P., Yu, K.K., Huo, Y.N., Meng, L., Wang, S., Wang, B.M., Du, M.W., Tian, X.L., et al. (2022). Thidiazuron Promotes Leaf Abscission by Regulating the Crosstalk Complexities between Ethylene, Auxin, and Cytokinin in Cotton. Int. J. Mol. Sci. **23**:20. 10.3390/ijms23052696.

Li, R.Z., Shi, C.L., Wang, X.Y., Meng, Y., Cheng, L.N., Jiang, C.Z., Qi, M.F., Xu, T., and Li, T.L.

(2021). Inflorescence abscission protein SlIDL6 promotes low light intensity-induced tomato flower abscission. Plant Physiol. **186**:1288-1301. 10.1093/plphys/kiab121.

Liang, Y., Jiang, C., Liu, Y., Gao, Y., Lu, J., Aiwaili, P., Fei, Z., Jiang, C.-Z., Hong, B., Ma, C., et al. (2020). Auxin regulates sucrose transport to repress petal abscission in Rose (Rosa hybrida). Plant Cell **32**:3485-3499. 10.1105/tpc.19.00695.

Lim, P.O., Woo, H.R., and Nam, H.G. (2003). Molecular genetics of leaf senescence in Arabidopsis. Trends Plant Sci. **8**:272-278. 10.1016/s1360-1385(03)00103-1.

Liu, X.T., Zhou, X.F., Li, D.D., Hong, B., Gao, J.P., and Zhang, Z. (2023a). Rose WRKY13 promotes disease protection to Botrytis by enhancing cytokinin content and reducing abscisic acid signaling. Plant Physiol. **191**:679-693. 10.1093/plphys/kiac495.

Liu, Z.J., Kong, X.Y., Long, Y.P., Liu, S.R., Zhang, H., Jia, J.B., Cui, W.H., Zhang, Z.M., Song, X.W., Qiu, L.J., et al. (2023b). Integrated single-nucleus and spatial transcriptomics captures transitional states in soybean nodule maturation. Nat. Plants. **9**:515-+. 10.1038/s41477-023-01387-z.

Long, Y.P., Liu, Z.J., Jia, J.B., Mo, W.P., Fang, L., Lu, D.D., Liu, B., Zhang, H., Chen, W., and Zhai, J.X. (2021). FlsnRNA-seq: protoplasting-free full-length single-nucleus RNA profiling in plants. Genome Biol. **22**:14. 10.1186/s13059-021-02288-0.

Meng, X.Z., Zhou, J.G., Tang, J., Li, B., de Oliveira, M.V.V., Chai, J.J., He, P., and Shan, L.B. (2016). Ligand-Induced Receptor-like Kinase Complex Regulates Floral Organ Abscission in Arabidopsis. Cell. Rep. **14**:1330-1338. 10.1016/j.celrep.2016.01.023.

Ortiz-Ramirez, C., Guillotin, B., Xu, X., Rahni, R., Zhang, S., Yan, Z., Araujo, P.C.D., Demesa-Arevalo, E., Lee, L., Van Eck, J., et al. (2021). Ground tissue circuitry regulates organ complexity in maize and Setaria. Science **374**:1247-1252. 10.1126/science.abj2327.

Patharkar, O.R., and Walker, J.C. (2015). Floral organ abscission is regulated by a positive feedback loop. Proc. Natl. Acad. Sci. U. S. A. **112**:2906-2911. 10.1073/pnas.1423595112.

Qin, Y., Sun, M.L., Li, W.W., Xu, M.Q., Shao, L., Liu, Y.Q., Zhao, G.N., Liu, Z.P., Xu, Z.P., You, J.Q., et al. (2022). Single-cell RNA-seq reveals fate determination control of an individual fibre cell initiation in cotton (Gossypium hirsutum). Plant Biotechnol. J. **20**:2372-2388. 10.1111/pbi.13918.

Reddy, G.V., and Meyerowitz, E.M. (2005). Stem-cell homeostasis and growth dynamics can be uncoupled in the Arabidopsis shoot apex. Science **310**:663-667. 10.1126/science.1116261.

Reichardt, S., Piepho, H.P., Stintzi, A., and Schaller, A. (2020). Peptide signaling for drought-induced tomato flower drop. Science **367**:1482-+. 10.1126/science.aaz5641.

Robatzek, S., and Somssich, I.E. (2001). A new member of the Arabidopsis WRKY transcription factor family, AtWRKY6, is associated with both senescence- and defence-related processes. Plant J. **28**:123-133. 10.1046/j.1365-313X.2001.01131.x.

Roberts, J.A., Elliott, K.A., and Gonzalez-Carranza, Z.H. (2002). Abscission, dehiscence, and other cell separation processes. Annu. Rev. Plant Biol. **53**:131-158. 10.1146/annurev.arplant.53.092701.180236.

Schaum, N., Karkanias, J., Neff, N.F., May, A.P., Quake, S.R., Wyss-Coray, T., Darmanis, S., Batson, J., Botvinnik, O., Chen, M.B., et al. (2018). Single-cell transcriptomics of 20 mouse organs creates a Tabula Muris. Nature **562**:367-+. 10.1038/s41586-018-0590-4.

Schwarz, I., Scheirlinck, M.T., Otto, E., Bartrina, I., Schmidt, R.C., and Schmulling, T. (2020). Cytokinin regulates the activity of the inflorescence meristem and components of seed yield in oilseed rape. J. Exp. Bot. **71**:7146-7159. 10.1093/jxb/eraa419.

Shi, C.L., Stenvik, G.E., Vie, A.K., Bones, A.M., Pautot, V., Proveniers, M., Aalen, R.B., and

Butenko, M.A. (2011). Arabidopsis Class I KNOTTED-Like Homeobox Proteins Act Downstream in the IDA-HAE/HSL2 Floral Abscission Signaling Pathway. Plant Cell **23**:2553-2567. 10.1105/tpc.111.084608.

Stenvik, G.E., Tandstad, N.M., Guo, Y., Shi, C.L., Kristiansen, W., Holmgren, A., Clark, S.E., Aalen, R.B., and Butenko, M.A. (2008). The EPIP peptide of INFLORESCENCE DEFICIENT IN ABSCISSION is sufficient to induce abscission in Arabidopsis through the receptor-like kinases HAESA and HAESA-LIKE2. Plant Cell **20**:1805-1817. 10.1105/tpc.108.059139.

Sun, G.L., Xia, M.Z., Li, J.P., Ma, W., Li, Q.Z., Xie, J.J., Bai, S.L., Fang, S.S., Sun, T., Feng, X.L., et al. (2022). The maize single-nucleus transcriptome comprehensively describes signaling networks governing movement and development of grass stomata. Plant Cell **34**:1890-1911. 10.1093/plcell/koac047.

Wang, D.H., Hu, X., Ye, H.Z., Wang, Y., Yang, Q., Liang, X.D., Wang, Z.L., Zhou, Y.F., Wen, M.M., Yuan, X.Y., et al. (2023a). Cell-specific clock-controlled gene expression program regulates rhythmic fiber cell growth in cotton. Genome Biol. **24**:28. 10.1186/s13059-023-02886-0.

Wang, L., and Zhang, Q.F. (2017). Boosting rice yield by Fine-Tuning SPL gene expression. Trends Plant Sci. **22**:643-646. 10.1016/j.tplants.2017.06.004.

Wang, L.Y., Deng, Y.S., Kong, F.J., Duan, B., Saeed, M., Xin, M., Wang, X.G., Gao, L.Y., Shen, G.F., Wang, J.H., et al. (2023b). Evaluating the effects of defoliant spraying time on fibre yield and quality of different cotton cultivars. J. Agric. Sci. **161**:12. 10.1017/s0021859623000151.

Wang, P.C., Zhang, J., Sun, L., Ma, Y.Z., Xu, J., Liang, S.J., Deng, J.W., Tan, J.F., Zhang, Q.H., Tu, L.L., et al. (2018). High efficient multisites genome editing in allotetraploid cotton (Gossypium hirsutum) using CRISPR/Cas9 system. Plant Biotechnol. J. **16**:137-150. 10.1111/pbi.12755.

Wendrich, J.R., Yang, B.J., Vandamme, N., Verstaen, K., Smet, W., Van de Velde, C., Minne, M., Wybouw, B., Mor, E., Arents, H.E., et al. (2020). Vascular transcription factors guide plant epidermal responses to limiting phosphate conditions. Science **370**:810-+. 10.1126/science.aay4970.

Wu, L., Ma, N., Jia, Y.C., Zhang, Y., Feng, M., Jiang, C.Z., Ma, C., and Gao, J.P. (2017). An Ethylene-Induced regulatory module delays flower senescence by regulating cytokinin content. Plant Physiol. **173**:853-862. 10.1104/pp.16.01064.

Xiao, H.M., Cai, W.J., Ye, T.T., Ding, J., and Feng, Y.Q. (2018). Spatio-temporal profiling of abscisic acid, indoleacetic acid and jasmonic acid in single rice seed during seed germination. Anal. Chim. Acta. **1031**:119-127. 10.1016/j.aca.2018.05.055.

Xu, J., Chen, L., Sun, H., Wusiman, N., Sun, W.N., Li, B.Q., Gao, Y., Kong, J., Zhang, D.W., Zhang, X.L., et al. (2019). Crosstalk between cytokinin and ethylene signaling pathways regulates leaf abscission in cotton in response to chemical defoliants. J. Exp. Bot. **70**:1525-1538. 10.1093/jxb/erz036.

Yeh, S.Y., Chen, H.W., Ng, C.Y., Lin, C.Y., Tseng, T.H., Li, W.H., and Ku, M.S.B. (2015). Down-Regulation of Cytokinin oxidase 2 expression increases tiller Number and improves rice yield. Rice **8**:13. 10.1186/s12284-015-0070-5.

Yu, Y.Q., Hu, H., Doust, A.N., and Kellogg, E.A. (2020). Divergent gene expression networks underlie morphological diversity of abscission zones in grasses. New Phytol. **225**:1799-1815. 10.1111/nph.16087.

Zeng, J.Y., Yan, X.Y., Bai, W.Q., Zhang, M., Chen, Y., Li, X.B., Hou, L., Zhao, J., Ding, X.Y., Liu, R.C., et al. (2022). Carpel-specific down-regulation of GhCKXs in cotton significantly enhances seed and fiber yield. J. Exp. Bot. **73**:6758-6772. 10.1093/jxb/erac303.

Zhang, L., Zhao, Y.L., Gao, L.F., Zhao, G.Y., Zhou, R.H., Zhang, B.S., and Jia, J.Z. (2012).

TaCKX6-D1, the ortholog of rice OsCKX2, is associated with grain weight in hexaploid wheat. New Phytol. **195**:574-584. 10.1111/j.1469-8137.2012.04194.x.

Zhang, M., Zeng, J.Y., Long, H., Xiao, Y.H., Yan, X.Y., and Pei, Y. (2017). Auxin regulates cotton fiber initiation via GhPIN-Mediated Auxin transport. Plant Cell Physiol. **58**:385-397. 10.1093/pcp/pcw203.

Zhang, W., Peng, K.X., Cui, F.B., Wang, D.L., Zhao, J.Z., Zhang, Y.J., Yu, N.N., Wang, Y.Y., Zeng, D.L., Wang, Y.H., et al. (2021). Cytokinin oxidase/dehydrogenase OsCKX11 coordinates source and sink relationship in rice by simultaneous regulation of leaf senescence and grain number. Plant Biotechnol. J. **19**:335-350. 10.1111/pbi.13467.

Zhao, J., Bai, W.Q., Zeng, Q.W., Song, S.Q., Zhang, M., Li, X.B., Hou, L., Xiao, Y.H., Luo, M., Li, D.M., et al. (2015). Moderately enhancing cytokinin level by down-regulation of GhCKX expression in cotton concurrently increases fiber and seed yield. Mol. Breed. **35**:11. 10.1007/s11032-015-0232-6.

Zhou, Y., Yan, A., Han, H., Li, T., Geng, Y., Liu, X., and Meyerowitz, E.M. (2018). HAIRY MERISTEM with WUSCHEL confines CLAVATA3 expression to the outer apical meristem layers. Science **361**:502-+. 10.1126/science.aar8638.

Zhu, X., Xu, Z., Wang, G., Cong, Y., Yu, L., Jia, R., Qin, Y., Zhang, G., Li, B., Yuan, D., et al. (2023). Single-cell resolution analysis reveals the preparation for reprogramming the fate of stem cell niche in cotton lateral meristem. Genome Biol. **24**:194. 10.1186/s13059-023-03032-6.